Resolving spatial heterogeneities in exhumation and surface uplift in Timor-Leste: Constraints on deformation processes in young orogens

Garrett W. Tate[1], Nadine McQuarrie[2], Douwe J. J. van Hinsbergen[3], Richard R. Bakker[4], Ron Harris[5], Sean Willett[4], Peter W. Reiners[6], Maria Giuditta Fellin[4], Morgan Ganerød[7], and Willem Jan Zachariasse[3]

[1]Geosciences, Princeton University, Princeton, New Jersey, USA, [2]Geology and Planetary Science, University of Pittsburgh, Pittsburgh, Pennsylvania, USA, [3]Department of Earth Sciences, Utrecht University, Utrecht, Netherlands, [4]Department of Earth Sciences, ETH Zurich, Zurich, Switzerland, [5]Department of Geological Sciences, Brigham Young University, Provo, Utah, USA, [6]Department of Geosciences, University of Arizona, Tucson, Arizona, USA, [7]Geological Survey of Norway, Trondheim, Norway

Abstract Although exhumation and surface uplift are important parameters in understanding orogenesis, the opportunity to measure both in close proximity is rare. In Timor-Leste (East Timor), deeply exhumed metamorphic rocks and piggyback deepwater synorogenic basins are only tens of kilometers apart, permitting direct relation of uplift and exhumation by comparing micropaleontology to thermochronology interpreted through one-dimensional thermal modeling. Foraminifera in two deepwater synorogenic basins suggest basin uplift from depths of 1–2 km to depths of 350–1000 m between 3.35 and 1.88 Ma. Thermochronologic sampling was conducted in the central mountain belt between these basins. Of four muscovite $^{40}Ar/^{39}Ar$ samples, one provides a reset age of 7.13 ± 0.25 Ma in the Aileu high-grade belt that suggests ~9–16 km of exhumation since that time. Eighteen zircon (U-Th)/He samples contain a group of reset ages in the Aileu Complex ranging from 4.4 to 1.5 Ma, which suggest exhumation rates of 1.0–3.1 mm/yr with 2.7–7.8 km of exhumation since these ages. Thirteen apatite (U-Th)/He ages in the Gondwana Sequence range from 5.5 to 1.4 Ma, suggesting 1–2 km of exhumation and defining a pattern of exhumation rates (ranging from 0.2 to 1.3 mm/yr) that positively correlates with average annual rainfall. Seven apatite fission track samples display varying degrees of partial resetting, with greatest resetting where apatite (U-Th)/He ages are youngest. Together, these data demonstrate extreme variability in surface uplift and exhumation over small spatial scales. We propose ongoing subsurface duplexing driven by subduction and underplating of Australian continental crust as the predominant driver for surface uplift and uplift-induced exhumation.

1. Introduction

Low-temperature thermochronology and paleoelevation (i.e., paleobathymetry or paleoaltimetry) analyses have each become valuable techniques in evaluating orogenic development, as they allow one to document exhumation and surface uplift respectively [e.g., *Fitzgerald et al.*, 1995; *Meulenkamp et al.*, 1994; *Poage and Chamberlain*, 2001; *Reiners and Brandon*, 2006]. Although still powerful when used separately, used together, these techniques elucidate the wavelength and the relative contributions of processes that control surface and rock uplift. For example, a broad wavelength signal of surface uplift derived from paleoaltimeters may suggest rock uplift and exhumation of a similarly broad wavelength, but unrecognized, focused zones of erosion could mask shorter wavelength changes in exhumation and possibly elevation [*Garzione et al.*, 2008; *Leier et al.*, 2013]. Similarly, exhumation constraints without estimates of surface uplift removes the ability to link structural thickening to changes in elevation and thus examine the control that surface elevation exerts on the geodynamic evolution of an orogen [*DeCelles et al.*, 2009; *Garzione et al.*, 2006]. Knowledge of the timing of surface uplift and emergence above sea level can constrain the permissible mechanisms of exhumation during early stages of orogenesis. Efforts to incorporate both thermochronology and paleoelevation data often require the extrapolation of data over tens to hundreds of kilometers, as paleoelevation indicators commonly within piggyback synorogenic basins are not often preserved near the exhumed units most useful for thermochronology. Regional extrapolation of these data assumes that patterns of exhumation and uplift remain consistent over these length scales. Although this assumption may hold as a time-integrated average over the life of a mature orogen, it overlooks the possibility that over short time periods, and for young orogens, exhumation and uplift could vary significantly over short length scales.

The island of Timor provides an excellent opportunity to examine the heterogeneity of uplift and exhumation in a convergent orogen. Timor is a young mountain belt with orogenesis beginning in the late Miocene [*Berry and McDougall*, 1986], and as such, preserves several klippen of the overthrust upper plate [*Carter et al.*, 1976] and piggyback basins of deepwater synorogenic deposits that record pre-uplift and early-uplift stages of evolution [*Haig and McCartain*, 2007]. Additionally, a variety of exhumed lower plate units are also exposed at the surface, including an unmetamorphosed foreland fold-thrust belt, a slate belt, and a phyllite-amphibolite grade belt [*Audley-Charles*, 1968]. All of these units are confined to an area of 120 by 80 km, providing an opportunity to examine the full history of Timor's orogenic development with minimal risk from errors associated with regional extrapolation. Furthermore, the varied terranes fortuitously preserved in this young orogen would likely be lost in the time-averaged signals of exhumation and uplift of a more mature orogen, allowing a unique opportunity to evaluate the mechanisms causing spatially variable uplift and exhumation for young orogens and over short time scales.

Much debate remains regarding the processes driving the structural development of Timor due to limited observations or more remote, regional data sets. *Haig and McCartain* [2007] use foraminifera from deepwater synorogenic marls to identify a phase of rapid surface uplift from lower bathyal (1–2 km) to middle bathyal (350–1000 m) depths between 3.35 and 3.12 Ma. This phase of rapid uplift was interpreted to be due to isostatic rebound after slab detachment [*Keep and Haig*, 2010] supported by an observed spatial gap in seismicity interpreted to be due to a tear in the downgoing slab [*Ely and Sandiford*, 2010; *Mccaffrey et al.*, 1985; *Sandiford*, 2008]. Arguments against this hypothesis include (1) surface uplift identified in a single basin may not be representative of the entire island, (2) tomographic studies image a continuous downgoing slab [*Fichtner et al.*, 2010; *Spakman and Hall*, 2010], and (3) GPS studies show continued convergence (and thus the possibility of subduction) between Timor and Australia at about 20 mm/yr [*Nugroho et al.*, 2009]. Observations of underthrust strata from the downgoing plate now exposed at the surface of Timor suggest that the orogen developed as a fold-thrust belt, with duplexing of thin Australian-affinity units below an overthrust lid of Banda Arc affinity [*Charlton et al.*, 1991; *Harris*, 1991; *Karig et al.*, 1987], providing a potential structural mechanism for thickening and uplift. However, without the ability to date the age of shortening, the relationship between shortening and uplift remains unknown. Accentuating this debate is the young, rapid uplift of coral terraces on Timor and on nearby islands that has been variously attributed to subsurface duplexing (for example *Cox* [2009], who notes that varying terrace uplift rates match the wavelength of structural antiforms and synforms) or to isostatic rebound following slab breakoff (for example *Ely et al.* [2011], who note the seismic gap below uplifted terraces on the island of Atauro).

Here we present new (U-Th)/He ages in zircon and apatite, new apatite fission track ages, and new muscovite ^{40}Ar/^{39}Ar ages from the central mountain belt of Timor-Leste in conjunction with two new micropaleontological data sets from preserved former deepwater synorogenic basins in Timor-Leste. The range in closure temperatures and wide aerial distribution of thermochronology samples highlight patterns of exhumation during both the early and late development of the orogen. The evaluation of deepwater synorogenic basins in both the foreland and hinterland of the orogen allows us to test the consistency of uplift signals across the island. Combined, these data sets constrain a detailed history of variable uplift and exhumation in space and time on Timor, provide opportunities to test previously proposed mechanisms of deformation on Timor, and demonstrate an extreme degree of heterogeneity of uplift and exhumation over small spatial scales.

2. Geologic Setting

The Timor mountain belt is a fold-thrust belt resulting from convergence between the Banda volcanic arc and the Australian continent [*Audley-Charles*, 1968] (see Figure 1). Prolonged convergence between the Australian margin and the Banda Arc has built the Timor orogen through structural repetition of Australian strata below Banda forearc units [*Harris*, 1991]. The Banda forearc is visible on the island of Timor as overthrust klippen consisting of metamorphic Banda forearc basement (primarily chloritized greenschist, graphitic phyllite, and amphibolite gneiss) and overlying volcanic and sedimentary units (including deep-marine turbidites, shallow-water carbonates, tuffs, and basalts) [*Harris*, 2006; *Standley and Harris*, 2009]. The décollement for the Banda forearc is the Bobonaro tectonic mélange, which contains meter- to kilometer-scale blocks of all units on Timor entrained within a matrix of Jurassic-age shales [*Harris et al.*, 1998]. Pre-Cretaceous age rocks, deposited in intracratonic basins of northern Australia [*Bird and Cook*, 1991], are duplexed below the Banda Arc klippe.
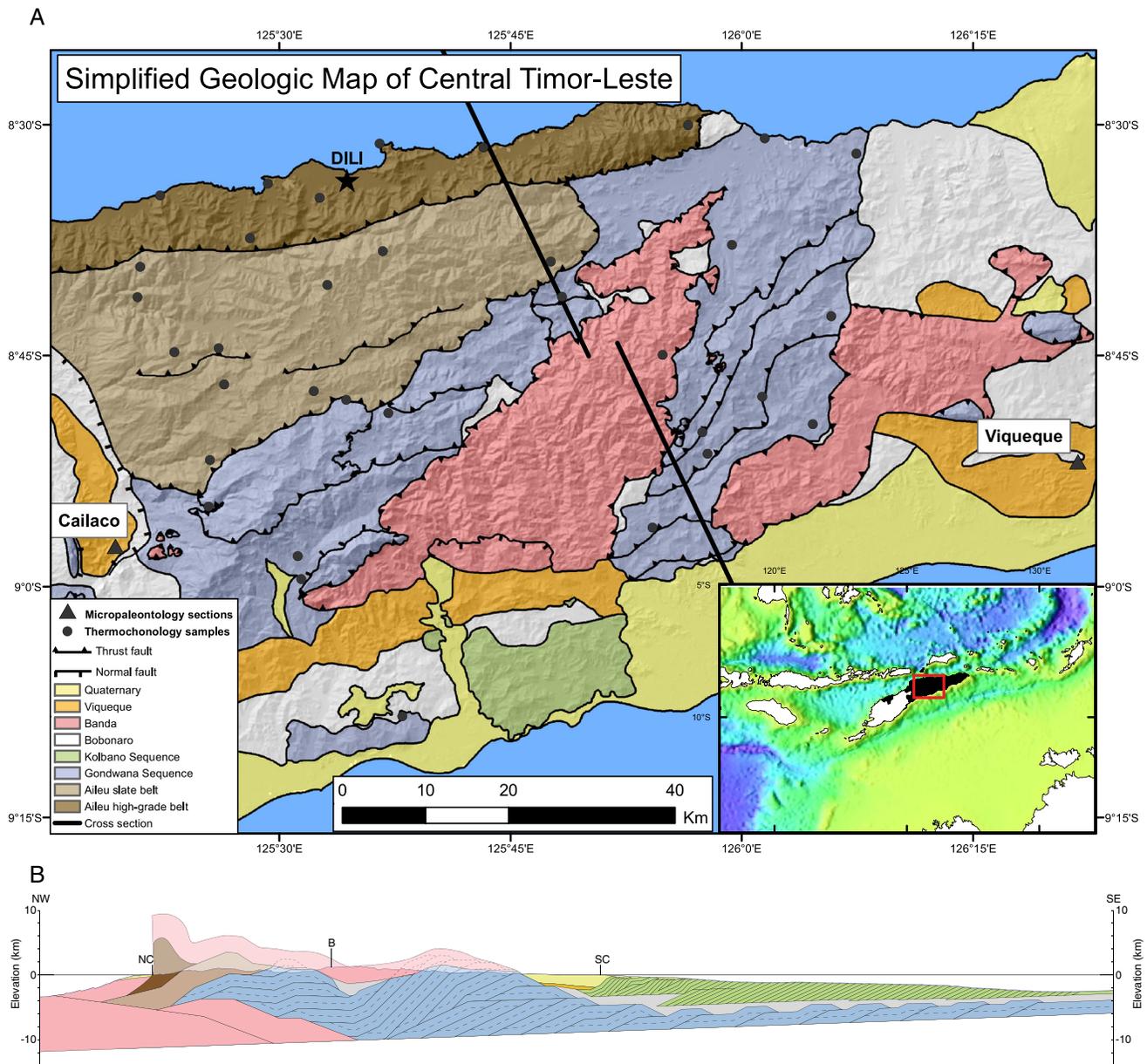
Figure 1. (a) Simplified structural map of central Timor-Leste. Within the area of thermochronology sampling mapping is from preliminary mapping by these authors. Outside of the thermochronology sampling area, mapping is compiled from previous mapping by *Audley-Charles* [1968], *Benincasa et al.* [2012], and *Duffy et al.* [2013]. Inset shows regional setting and surrounding bathymetry (from National Geophysical Data Center, NOAA), with Timor-Leste in black and study area outlined in red. (b) Simplified cross section of Timor along section trend in Figure 1a. Duplexing of Gondwana Sequence fills majority of wedge. Gap between Kolbano Sequence thrust belt and leading edge of Banda overthrust klippe allows for deposition of Viqueque Sequence directly on Bobonaro mélange. NC = north coast, SC = south coast, B = break in section.

In the foreland (southeastern facing) and central portions of the island, the duplex contains Permian-Jurassic age carbonates and clastics of the Gondwana Sequence [*Carter et al.*, 1976], and in the hinterland, the Permian-age Aileu Metamorphic Complex is interpreted to be structurally repeated [*Prasetyadi and Harris*, 1996]. The Aileu Complex has undergone variable degrees of metamorphism. Our preliminary mapping (Figure 1) divides the Aileu Complex based on metamorphic grade into a wide slate belt to the south (which we refer to as the Aileu slate belt) and a phyllite to schist belt along the north coast (which we refer to as the Aileu high-grade belt). The metamorphic grade of the Aileu high-grade belt has previously been observed to decrease from east to west, as mapped faults near the city of Dili separate amphibolite-grade units in the eastern high-grade belt from the western high-grade belt that is dominated by phyllites [*Berry and Grady*, 1981;

Prasetyadi and Harris, 1996]. The post-Cretaceous Australian-affinity section consists of the passive margin Kolbano Sequence, dominated by Cretaceous calcilutites onshore in Timor-Leste [*Audley-Charles*, 1968] but also including shale, chert, sandstone, and other limestone units [*Sawyer et al.*, 1993] as young as 9.8 Ma [*Keep and Haig*, 2010]. The Kolbano Sequence is deformed in a foreland fold-thrust belt along the Bobonaro décollement at the leading edge of the Banda Terrane and is mostly offshore in Timor-Leste except for isolated exposures near the south coast [*Carter et al.*, 1976; *Charlton et al.*, 1991; *Harris*, 2006; *Sawyer et al.*, 1993].

The Viqueque Sequence (part of the Banda Orogen Sequence of *Roosmawati and Harris* [2009]) is a succession of deepwater synorogenic Miocene to Pliocene deposits preserved in isolated piggyback basins across the island. The basal portion of the sequence consists of chalky marl and limestone, whereas the upper portion is a coarsening-upward succession of clay and turbidites containing clasts of Banda and Gondwana Sequence units as well as fossil wood [*Audley-Charles*, 1968; *Carter et al.*, 1976; *Desmet et al.*, 1990; *Haig and McCartain*, 2007; *Nguyen et al.*, 2013]. These synorogenic sediments are deposited unconformably on the Bobonaro mélange [*Desmet et al.*, 1990; *Haig and McCartain*, 2007]. Other units are typically structurally above the Bobonaro mélange (the Banda Terrane in the hinterland and the Kolbano Sequence in the foreland), but these units are missing in locations of preserved Viqueque Sequence basins. The absence of both the Banda Terrane and the Kolbano Sequence between the Viqueque Sequence and the Bobonaro Mélange requires a mechanism to subaqueously remove these units after the development of the Bobonaro Mélange and before the deposition of the deep marine basal Viqueque Sequence (dated by *Haig and McCartain* [2007] at 5.6–5.2 Ma).

Stratigraphic observations have previously been used to support a late Miocene age for the initiation of collision at Timor. *Keep and Haig* [2010] suggest that collision began after 9.8 Ma, which is the age of the youngest preserved outcrop of the precollisional passive margin Kolbano Sequence. Additionally, basal Viqueque Sequence limestones deposited on the Bobonaro mélange, which formed during orogenesis [*Harris et al.*, 1998], are dated at 5.6–5.2 Ma [*Haig and McCartain*, 2007] indicating that orogenesis was proceeding by this time.

Thermochronology within the Aileu high-grade belt has also been used to support the interpretation of initial collision at Timor by the late Miocene. *Berry and McDougall* [1986] find a muscovite ^{40}Ar/^{39}Ar plateau of 5.36 ± 0.10 Ma in the Aileu high-grade belt [*Berry and McDougall*, 1986], strongly suggesting that orogenesis and exhumation were proceeding by this time. Additionally, *Berry and McDougall* [1986] described a hornblende ^{40}Ar/^{39}Ar sample in the Aileu high-grade belt with an "essentially flat release pattern" providing a "good estimate" Ar closure age of 7.5 Ma, as well as a few other samples with hornblende ^{40}Ar/^{39}Ar spectra suggesting substantial Ar loss at ~7.5–8 Ma, providing some support that exhumation may have been proceeding as early as 7.5 Ma. There is, however, some debate over whether these ages and this region of the Aileu high-grade belt are associated with processes within the Banda forearc [*Audley-Charles*, 2011; *Ely et al.*, 2014; *Kaneko et al.*, 2007] or represent the initial collision of the distal-most Australian margin [*Berry and McDougall*, 1986; *Harris and Long*, 2000; *Standley and Harris*, 2009; *Valenza et al.*, 2013]. *Ely et al.* [2014] used a detrital zircon peak at 290 Ma and hornblende ^{40}Ar/^{39}Ar ages of 10–6 Ma to argue that the Aileu high-grade belt belongs to terranes such as the Sula Spur that rifted from Australia in the Mesozoic and were incorporated in the Banda forearc before collision with the Australian margin. We note, however, that although the Sula Spur is a permissible sediment source for the protoliths of the Aileu high-grade belt, rifting of the Sula Spur away from the Australian margin in the Mesozoic does not necessitate rifting of the Aileu high-grade belt protoliths away from Australia as well, as deposition of those protoliths predates rifting. Sediments of the Gondwana Sequence demonstrate a similar modern separation from their sediment source, as paleocurrent directions from the north [*Bird and Cook*, 1991] and detrital zircon peaks from 254 to 385 Ma [*Zobell*, 2007] also require source regions that were rifted from Australia in the Mesozoic. We currently prefer an interpretation that includes the protolith of the Aileu high-grade belt as part of the distal Australian margin. This interpretation would suggest that these muscovite and hornblende ^{40}Ar/^{39}Ar ages are associated with initial collision at Timor. If instead these ages are indicative of an earlier collision event between Sula Spur fragments and the Banda Arc, collision at Timor still must have begun well before 5.6–5.2 Ma, as significant deformation must have preceded the deposition of the Viqueque Sequence to allow for development of the Bobonaro mélange prior to deposition of these synorogenic sediments.

Some have argued for a younger, Pliocene age of collision, such as *Audley-Charles* [2011] who suggests that Banda Arc volcanism until 3 Ma precludes collision of the Australian margin with the Banda Arc before about 4 Ma. However, an interpretation of early subduction of the distal-most Australian margin is
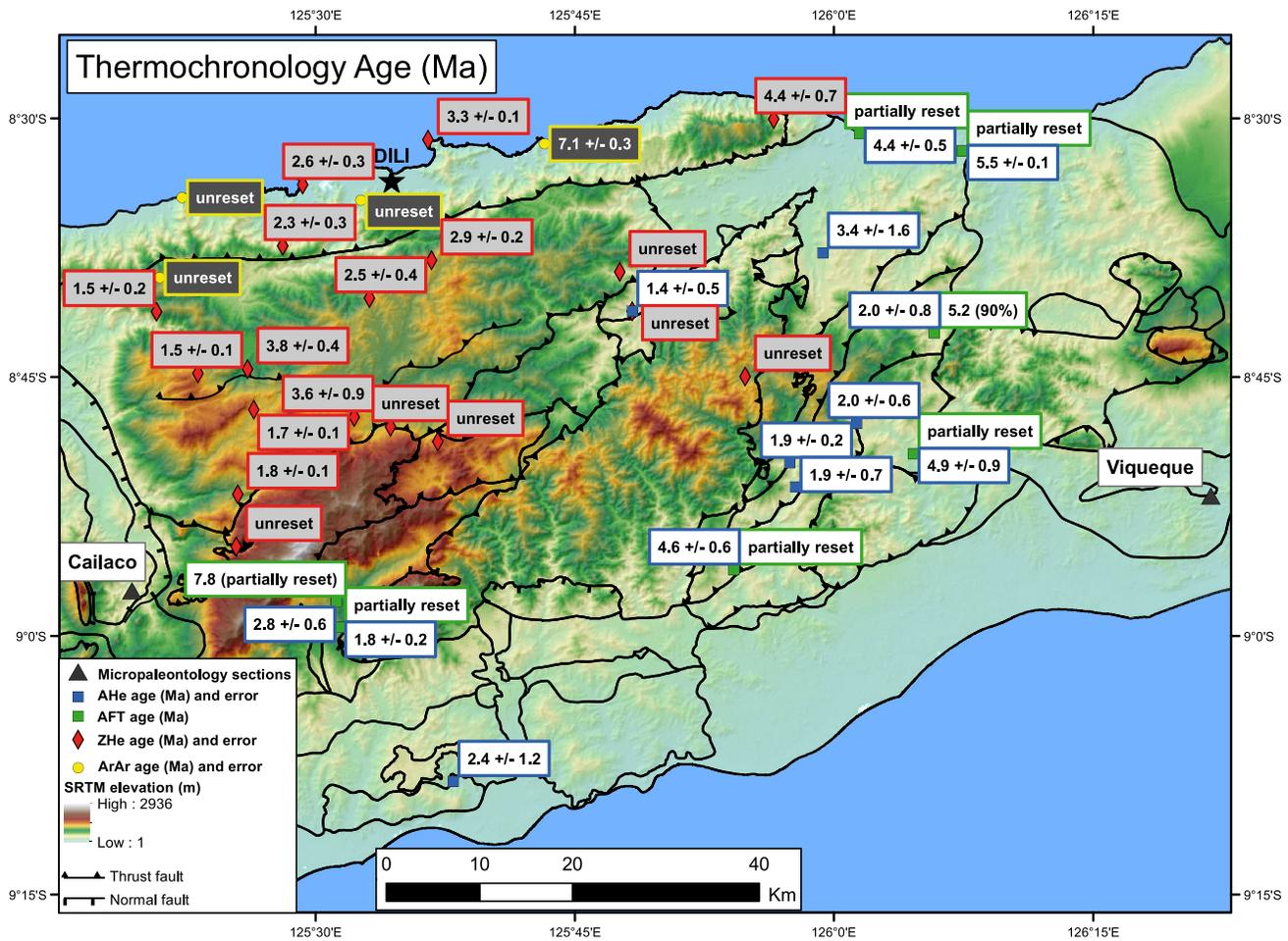
Figure 2. AHe, AFT, ZHe, and MAr thermochronology data (age and 2σ error) shown with elevation, mapped contacts and faults, and synorogenic section locations. AFT ages are all partially reset, with ages shown for two samples noted in the text (7.8 Ma pooled age in the western map area and 5.2 Ma 90% population age in the eastern map area).

supported by helium and lead isotopic signals within Banda Arc volcanics suggesting contamination with continental material from 7 to 3 Ma [*Elburg et al.*, 2004; *Hilton and Craig*, 1989]. Furthermore, the process of structural repetition that has built the Timor orogen [*Harris*, 1991] suggests the incorporation of Australian units from a paleomargin extending hundreds of kilometers that has been subducted at Timor [*Keep and Haig*, 2010; *Tate et al.*, 2010]. It is important to note that we refer to collision at Timor as a process of protracted deformation that has occurred over several Myr, noting the structural repetition that has built the orogen [*Harris*, 1991] as well as GPS data that describe ongoing convergence between Timor and Australia [*Nugroho et al.*, 2009].

First emergence of an island at Timor is suggested to be shortly before 4.45 Ma [*Nguyen et al.*, 2013], as indicated by an increase in clastic sedimentation and an increased contribution from mangrove and lowland rainforest flora in the pollen record.

3. Methods

3.1. (U-Th)/He Thermochronology

We obtained 18 new zircon (U-Th)/He (ZHe) and 13 new apatite (U-Th)/He (AHe) ages from 30 samples in central Timor-Leste (Figure 2). Of these, 15 samples were taken from sandstones within the Gondwana Sequence, 14 samples were taken from quartzites in the Aileu Complex, and one sample was taken from the Banda Terrane.

Each 6–8 kg sample was ground and separated for apatite and zircon using magnetic and heavy liquid separation techniques. Samples were processed at the University of Arizona Radiogenic Helium Dating Laboratory. Three zircons were picked from each of 18 samples, each grain with a minimum width of 60 μm. Three to five apatites (depending upon availability) were picked from each of 13 samples, each grain with a minimum width of 60 μm. When completely inclusion-free apatites were not present, some apatites were used that contained one to three 5 μm-diameter inclusions. Individual grains were degassed by laser heating, and U-Th-Sm content was measured by Inductively Coupled Plasma Mass Spectrometry. For further detail on the methods used, see the supporting information (Text S1) and *Reiners et al.* [2004].

3.2. Apatite Fission Track Thermochronology

Seven samples from sandstones within the Gondwana Sequence were analyzed for apatite fission track (AFT) thermochronology. Apatites were obtained using standard magnetic and heavy liquid separation techniques. Fission track analysis was performed using the external detector method combined with zeta-age calibration [*Hurford and Green*, 1983]. Grain mounting and track counting were performed at ETH in Zurich, Switzerland. Samples were irradiated at the TRIGA reactor of the Oregon State University Radiation Center, with a nominal neutron fluence of 1e16 n cm^{-2} for a total of 37.75 h.

3.3. ^{40}Ar/^{39}Ar Thermochronology

Four quartzite samples were analyzed for muscovite ^{40}Ar/^{39}Ar (MAr) thermochronology. All samples contained quartz grains (70–97%), muscovite (30–2%), and minor (10% or less) amounts of biotite, iron-rich opaque minerals, and lithics. One sample was from amphibolite-grade units in the eastern Aileu high-grade belt (TL11-393), two samples were within phyllite-grade units of the western Aileu high-grade belt (TL11-323 and TL11-397), and one was a quartzite sample from the northern area of the Aileu slate belt (TL11-338). Each sample had a grain size of ~200 μm. White mica separates were obtained using magnetic and heavy liquid separation techniques. Mineral grains were picked avoiding grain coatings and inclusions. Standard analytical techniques were used, with irradiation performed at Institutt for Energiteknikk, Kjeller, Norway, and degassing and mass spectrometry performed at the Geological Survey of Norway, Trondheim. For further detail on the methods used, see the supporting information and *Ganerød et al.* [2011].

3.4. Thermal Modeling

Thermochronologic data were modeled to determine permissible exhumation rates using the one-dimensional thermal, exhumation model of *Willett and Brandon* [2013]. The models account for an advecting geothermal gradient due to hot rock motion toward the surface as well as the dependence of closure temperature on cooling rate. Kinematic parameters are listed in Table S1 and match those in *Robbins* [1972], *Hames and Bowring* [1994], *Ketcham et al.* [1999], *Farley* [2002], *Reiners* [2005], and *Reiners and Brandon* [2006]. Varying closure temperatures for these systems are included in the models using T_{c10}, the closure temperature for a cooling rate of 10°C/Myr. Exhumation rates and exhumation magnitudes are determined for the time period since cooling through the closure temperature at the given sample age. The time of initiation of exhumation (t_1) is set at 7.1 Ma for all (U-Th)/He and AFT models, as our reset MAr age of 7.1 ± 0.3 Ma (see MAr results below) suggests that exhumation on Timor began at least by this time. We use 7.5 Ma for t_1 in MAr models, as exhumation must start slightly before the closure age of 7.1 Ma. *Berry and McDougall* [1986] reported one hornblende ^{40}Ar/^{39}Ar age of 7.5 Ma in samples from the Aileu high-grade belt, lending support that exhumation may have begun by 7.5 Ma. (Models for (U-Th)/He using t_1 = 7.5 Ma differ from the t_1 = 7.1 Ma models by only about 2% in both exhumation rate and kilometers of exhumed material.) Following the procedures in *Willett and Brandon* [2013], mean local elevation is averaged over circles with radius of π times the estimated closure depth as the thermal signal from the rugged surface topography is expected to decay with depth (a 4 km radius is used for AHe models, 9 km radius for AFT models, 10 km radius for ZHe models, and 22 km radius for MAr models). Surface temperature follows modern-day temperatures of 27°C at sea level decreasing 6°C per km of elevation [*Timor-Leste Ministry of Agriculture*, 2012].

Models of exhumation require some constraint on either the modern or pre-exhumation geothermal gradient. Data on modern geothermal gradients on Timor are sparse and restricted to wells along the south coast of Timor. Three wells along the southern coast of Timor suggest modern geothermal gradients of 25–30°C/km, and one well shows a geothermal gradient of 15°C/km in the upper 1200 m and 30°C/km below 1200 m [*Harris et al.*, 2000]. In these regions only the lowest-temperature thermochronometers (AHe) are reset,

whereas the exposure of reset ZHe with similar ages in other areas suggests much faster exhumation that (through advection of heat to the surface) would result in much higher geothermal gradients. With the lack of modern geothermal gradient constraints in regions of widely differing exhumation magnitudes, we seek instead to use reasonable constraints on the pre-exhumation geothermal gradient. The large majority of the orogenic wedge is built through underplating and duplexing of units from the subducting Australian passive margin. The stacking of cold upper sedimentary units suggests that the geothermal gradient after the orogenic wedge has built but before exhumation begins would be below the geothermal gradient of the undeformed passive margin. We use 32°C/km for the pre-deformation passive margin geothermal gradient (matching that observed today on the Australian passive margin [*O'Brien et al.*, 1996]). We use 15°C/km for the minimum pre-exhumation geothermal gradient, based on the observed geothermal gradient in the upper 1.2 km of the Banli-1 well near the southern coast of Timor [*Harris et al.*, 2000] where there is duplexing of units from the subducting Australian passive margin but little exhumation has occurred. A similar geothermal gradient of 19°C/km to well bottom at 1.2 km is observed to in the Savu-1 well just off the north coast of Savu [*Kenyon and Beddoes*, 1977], in a position that has deformed similarly to the retrowedge of the north coast of Timor [*Harris*, 2011; *Harris et al.*, 2009]. We present two primary sets of models, one producing 32°C/km and another producing 15°C/km pre-exhumation geothermal gradients, that will provide lower and upper bounds, respectively, for exhumation rate and exhumation magnitude. Thermal models producing 25°C/km pre-exhumation geothermal gradients are presented as well. These may be more appropriate as an upper bound on exhumation for systems with larger exhumation magnitudes (ZHe and MAr), as the lowest gradient of 15°C/km has only been observed as deep at 1.2 km [*Harris et al.*, 2000].

3.5. Micropaleontology

Two stratigraphic sections of the Viqueque Sequence in Timor-Leste, one near the town of Viqueque (the type section of the Viqueque Sequence) and another south of the town of Cailaco (in the Marobo basin of *Duffy et al.* [2013]), were sampled for planktonic foraminiferal biostratigraphy and paleobathymetry using benthic foraminifers (see Figure 1 for location and Figure 3 for stratigraphic sections). Samples were taken approximately every 0.9 m in the basal pelagic limestone, every 1.8 m in the lower marl overlying this pelagic limestone, and every 2–3 m in shale units within the upper member of interbedded turbiditic sandstones and shales, except in nonexposed intervals. Subsequently, every third of 122 samples from the Viqueque type section and every second of 78 samples from the Cailaco section were placed in water for several days to allow for disaggregation (water was admixed by low concentrations of hydrogen peroxide for samples from basal limestones that did not adequately disaggregate in water). Samples were then washed through 600 and 125 μm sieves after which the residues of the 600–125 μm fraction were used for analysis. Age control on both sections is derived from importing ages for highest and lowest occurrences of age diagnostic planktonic foraminiferal species using the biochronologies of *Lourens et al.* [2004] and *Wade et al.* [2011]. Paleodepth estimates for both sections are based on the presence or absence (and relative abundance to planktonic forams) of those benthic foraminiferal species whose modern representatives show optimum occurrences within specific water depth intervals, such as those published by *Van Marle* [1988, 1989, 1991] and by *van Hinsbergen et al.* [2005].

4. Results

4.1. Apatite (U-Th)/He

Results from AHe analyses are included in Table S1 and are shown in Figure 2. Samples processed for AHe generally produce single-grain ages younger than 6 Ma and provide weighted mean ages ranging from 1.4 to 5.5 Ma. Most samples displayed significantly more variation of single-grain ages than ZHe analyses, and several anomalously high or low ages were removed from weighted mean analysis because of extremely low U concentration (noted in Table S1). In sample TL11-254, an anomalous single-grain age of 0.6 Ma was removed because of an extremely abraded grain morphology, and an anomalous age of 13.7 Ma was also removed on suspicion of He implantation (as this is much older than estimates for the beginning of orogenesis on Timor). Additionally, samples TL10-229 and TL10-314 displayed a positive age-eU correlation, suggesting significant time spent in the partial retention zone during cooling [*Flowers et al.*, 2008]. Because of this correlation, we removed anomalously old single-grain ages of 5.7 Ma and 7.8 Ma when calculating weighted means for TL10-229 and TL10-314, respectively, as those single-grain ages are likely only partially reset.
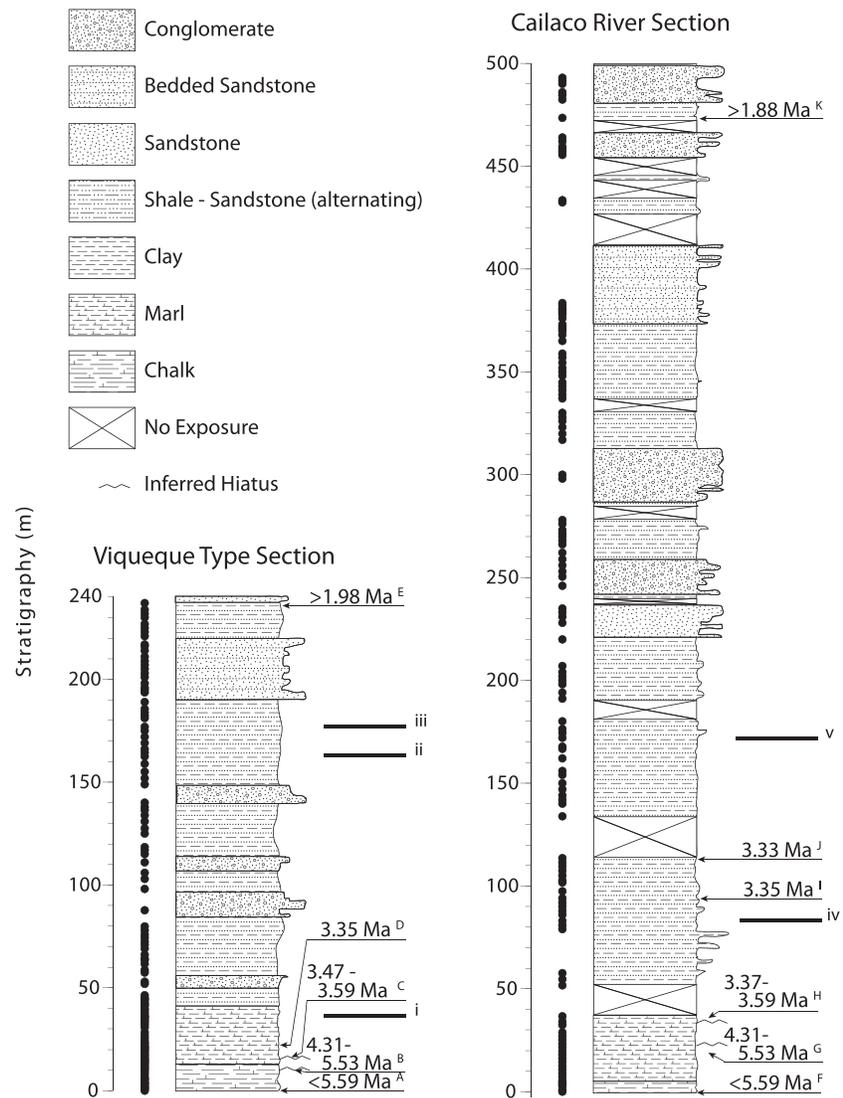
Figure 3. Stratigraphic logs of Viqueque type section and Cailaco River section. Sample levels are denoted with black dots. Significant horizons are labeled, noted below: Viqueque Type Section: (A) base younger than 5.59 Ma due to presence of *Globorotalia tumida* according to *Lourens et al.* [2004], 5.57 Ma in *Wade et al.* [2011]; (B) hiatus between 5.53 and 4.31, simultaneous first occurrence (FO) of *Sphaeroidinella dehiscens* and *Globorotalia crassaformis*; (C) second Hiatus between 3.59 and 3.47 Ma, simultaneous last occurrence (LO) of *Globoquadrina altispira* and representatives of *Sphaeroidinellopsis*; (D) 3.35 Ma FO of *Globorotalia toaensis*; (E) top older than 1.98 Ma due to presence of *Globigerina apertura*, *Globigerinoides obliquus*, and *Globigerinoides obliquus extremus*; (i) lowest presence of occasional middle bathyal species (*Uvigerina peregrina* and *Sphaeroidina bulloides*); (ii) lowest presence of other middle bathyal species (*Cibicides pseudoungarianus* and *Hyalinea balthica*); (iii) highest presence of lower bathyal species. Cailaco River section: (F) base younger than 5.59 Ma due to presence of *Globorotalia tumida* according to *Lourens et al.* [2004], 5.57 Ma in *Wade et al.* [2011]; (G) hiatus between 5.53 and 4.31, simultaneous FO of *Sphaeroidinella dehiscens* and *Globorotalia crassaformis*; (H) second hiatus between 3.59 and 3.47 Ma, simultaneous LO of *Globoquadrina altispira* and representatives of *Sphaeroidinellopsis*; (I) 3.35 Ma FO of *Globorotalia toaensis*; (J) 3.33 Ma FO of *Globigerinoides fistulosis*; (K) top older than 1.88 Ma, highest occurrence of *Globigerinoides fistulosis*; (iv) lowest occasional occurrence of middle bathyal species; (v) complete transition to middle bathyal species above 172 m.

Samples from the eastern map area follow a pattern that is symmetric about the mountain axis, with ages of 4.4 ± 0.5 Ma and 5.5 ± 0.1 Ma on the north coast, four ages of about 2.0 Ma in the south-central portion of the range, and 4.6 ± 0.6 and 4.9 ± 0.9 Ma in the southern foothills.

Outside of the eastern map area, there is an age of 1.4 ± 0.5 Ma in the hinterland exposures of the Gondwana Sequence, ages of 1.8 ± 0.2 and 2.8 ± 0.6 Ma along the central axis in the southwest map area, and an age of 2.4 ± 1.2 Ma near the southwest coast.

4.2. Zircon (U-Th)/He

Results from ZHe analyses are included in Table S1 and are shown in Figure 2. ZHe ages fall into two distinct groups, those younger than 5 Ma and those significantly older. The majority of grain ages within the Aileu high-grade and Aileu slate belts are younger than 5.0 Ma and range to as young as 1.4 Ma. At the far eastern end of the Aileu high-grade belt on the north coast, sample TL10-10 has a weighted mean ZHe age of 4.4 ± 0.7 Ma and ages progressively decrease in the Aileu high-grade belt toward the west to 2.3 ± 0.3 Ma. ZHe ages in the Aileu slate belt show a similar younging toward the west, with weighted mean sample ages in the central region about 3.0 Ma and ages of 1.5 to 1.8 Ma near the western edge of the slate belt. We note that for each of samples TL10-374, TL10-392, TL11-217, TL11-218, and TL11-282, two consistent single-grain ZHe ages were accompanied by one much older grain. In TL10-374, the grain with an age of 10.6 Ma was coated in orange material and likely influenced by He implantation. The older single-grain ages in TL10-392, TL11-217, TL11-218 and TL11-282 do not correlate with any unusual grain characteristic. It is possible that the heterogeneity of single-grain ages in samples along the western range front denotes a complex cooling history or significant time spent in the partial retention zone, but the lack of any correlation between age and grain size or effective uranium concentration leads us to believe that these older grain ages are simply affected by implantation.

The remaining ZHe ages are significantly older than 9.8 Ma, the earliest estimate of initial collision [*Keep and Haig*, 2010]. Sample TL11-405 from the Lolotoi Complex (forearc basement of the overthrust Banda Arc [*Standley and Harris*, 2009]) gives three consistent grain ages about a weighted mean of 25.7 ± 1.5 Ma. This age is younger than K/Ar and ^{40}Ar/^{39}Ar hornblende, muscovite, and biotite ages of 31–38 Ma in the Mutis Complex (the corollary to the Lolotoi Complex in West Timor) [*Harris*, 2006] and appears to record a shallower part of the exhumational history of the pre-collisional Banda forearc basement. Five other samples, TL10-126, TL11-111, TL11-130, TL11-219, and TL11-249, have single-grain ages varying over tens or hundreds of Ma. All single-grain ages are younger than the Permian to Jurassic age of deposition. These ages could reflect partial resetting of the ZHe system during orogenesis since the Miocene, or they could simply reflect the thermal history of the precollisional passive margin. These samples are all located closer to the foreland than the samples with young (<5.0 Ma) ages discussed above and are located in the southernmost Aileu slate belt and northernmost Gondwana Sequence duplex.

4.3. Apatite Fission Track

Results from AFT analyses are included in Table S1 and ages are shown in Figure 2. Samples evaluated for apatite fission track display varying degrees of partial annealing, with the degree of annealing showing a strong inverse correlation with AHe age. Samples from the northern and southern foothills of the eastern map area are only partially reset and contain numerous Mesozoic single-grain ages. Single-grain analyses within these samples also display a weak correlation between age and D_{par} (mean etched track diameter parallel to the *c* axis), indicating significant time spent in the partial annealing zone [*Donelick et al.*, 2005]. Samples along the central mountain axis display a much greater degree of resetting. HeFTy [*Ketcham*, 2005] models of track length distributions and AHe age for both samples TL10-208 and TL11-61 suggest residence of samples at 100–110°C since the Cretaceous and rapid exhumation from ~110°C to 20°C since 5 Ma (Figure 4). Additionally, BINOMFIT [*Brandon*, 2002] models of age populations within sample TL11-61 find that 90% of grains are represented by a population centered around 5.2 Ma. Apatite fission track analyses therefore indicate that more exhumation has occurred in Gondwana Sequence units in the central mountain axis compared to the northern and southern foothills and that rapid exhumation has occurred since ~5 Ma.

4.4. Mica ^{40}Ar/^{39}Ar

Results from MAr analyses are included in Table S1 and Figure 5, and ages are shown in Figure 2. (The raw data corrected for blanks can be found in the supporting information.) Sample TL11-393 in the eastern Aileu high-grade belt provided three stable degassing steps, yielding a spectrum weighted mean plateau age of 7.13 ± 0.25 Ma with an MSWD of 0.01. The inverse isochron age using these three steps was 7.0 ± 1.8 Ma, with an MSWD of 0.001 and an intercept of 302.75 ± 59.74. The spectrum outside
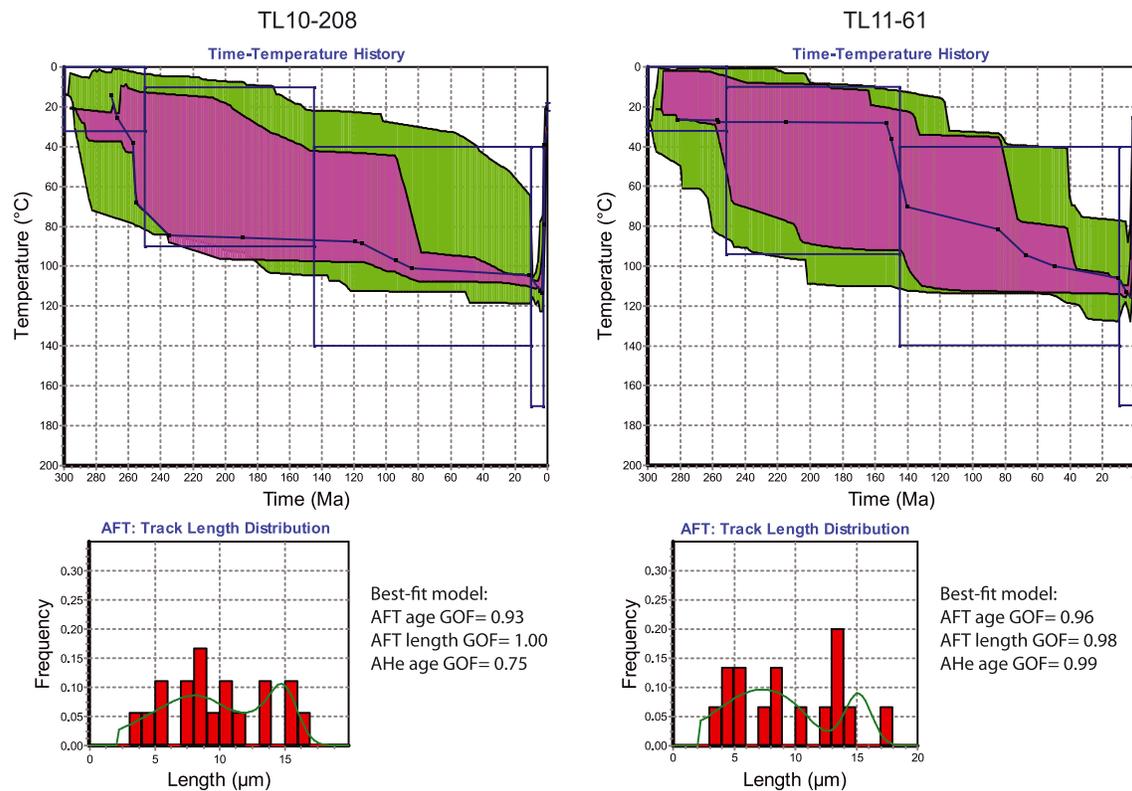
Figure 4. (a) Results from HeFTy modeling of AFT and AHe data from sample TL10-208. (b) Results from HeFTy modeling of AFT and AHe data from sample TL11-61. Envelope of acceptable fits shown in green, good fits shown in purple, and best fit shown by line. In both models, note long residence up to 100-110°C and rapid exhumation since 5 Ma.

of the three stable steps has a saddle shape and the inverse isochron intercept has large uncertainty, so there is a possibility that the sample possesses excess [40]Ar.

Sample TL11-397 in the central Aileu high-grade belt displayed a saddle-shaped degassing spectrum indicative of excess [40]Ar. The central portion of this spectrum yields an age of 55.9 ± 14.9 Ma. This old age indicates very little loss of [40]Ar during orogenesis on Timor.

Sample TL11-323 in the western Aileu high-grade belt displayed a saddle-shaped degassing spectrum indicative of excess [40]Ar. The most stable portion of the degassing spectrum consists of six steps that yield an age of 9.68 ± 1.12 Ma. Considering the great scatter in degassing steps (as indicated by the MSWD of 340.9), it is possible that an event younger than 9.68 Ma was not hot enough at this location to completely reset the system and caused only partial loss of radiogenic [40]Ar.

Sample TL11-338, about 9 km south of sample TL11-323 and to the south of the phyllite-slate boundary, displayed a staircase pattern in the degassing spectrum that is indicative of partial loss of radiogenic [40]Ar. The first degassing step is youngest and is dated at 15.34 ± 0.94 Ma, and the last degassing step is oldest at 164.41 ± 7.23 Ma. It is likely that an event at 15 Ma or younger heated the sample to temperatures high enough to only partially reset the system.

The pattern of [40]Ar/[39]Ar ages generally correlates with metamorphic grade. The eastern portion of the Aileu high-grade belt where sample TL11-393 is found is dominated by amphibolite-grade lithologies [*Berry and Grady*, 1981; *Prasetyadi and Harris*, 1996]. The central and western portion of the Aileu high-grade belt is dominated by lower-grade phyllites [*Prasetyadi and Harris*, 1996]. The degassing spectra for samples from these rocks (TL11-397 and TL11-323) do not display any stable plateaus. TL11-338 (south of TL11-323 and in the slate belt) has a total fusion age and a youngest degassing step that are older than those of TL11-323, suggesting a lower peak temperature in the slate belt at TL11-338 during orogenesis.
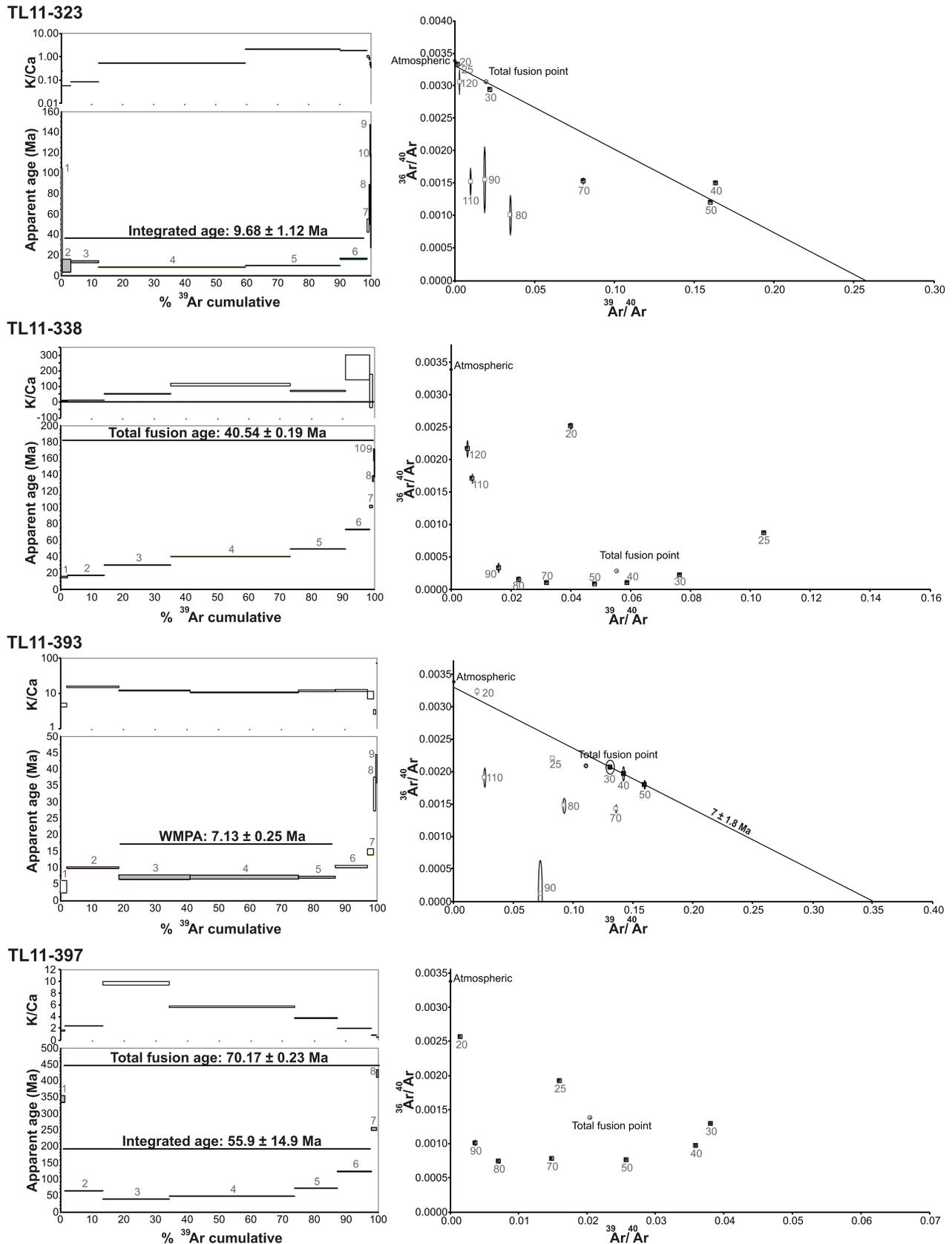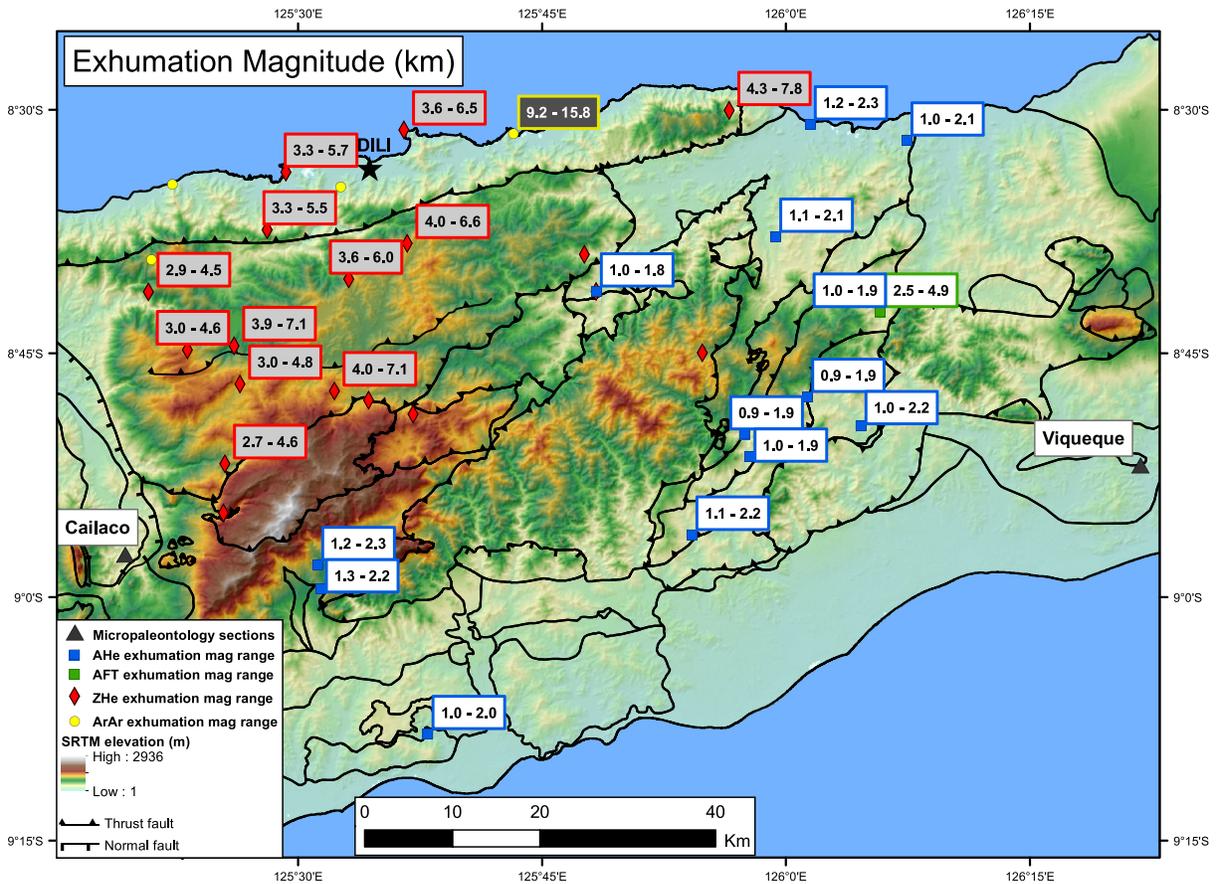
Figure 5. MAr degassing spectra and isochron plots for each sample. Plateau ages included for most stable degassing steps.

Figure 6. Range of exhumation magnitudes in thermal modeling of thermochronology data. Magnitudes only represent thickness of exhumed material since time of closure. The single AFT model is for an age of 5.2 Ma representing 90% of the sample grains and represents a reasonable upper bound for exhumation of this sample.
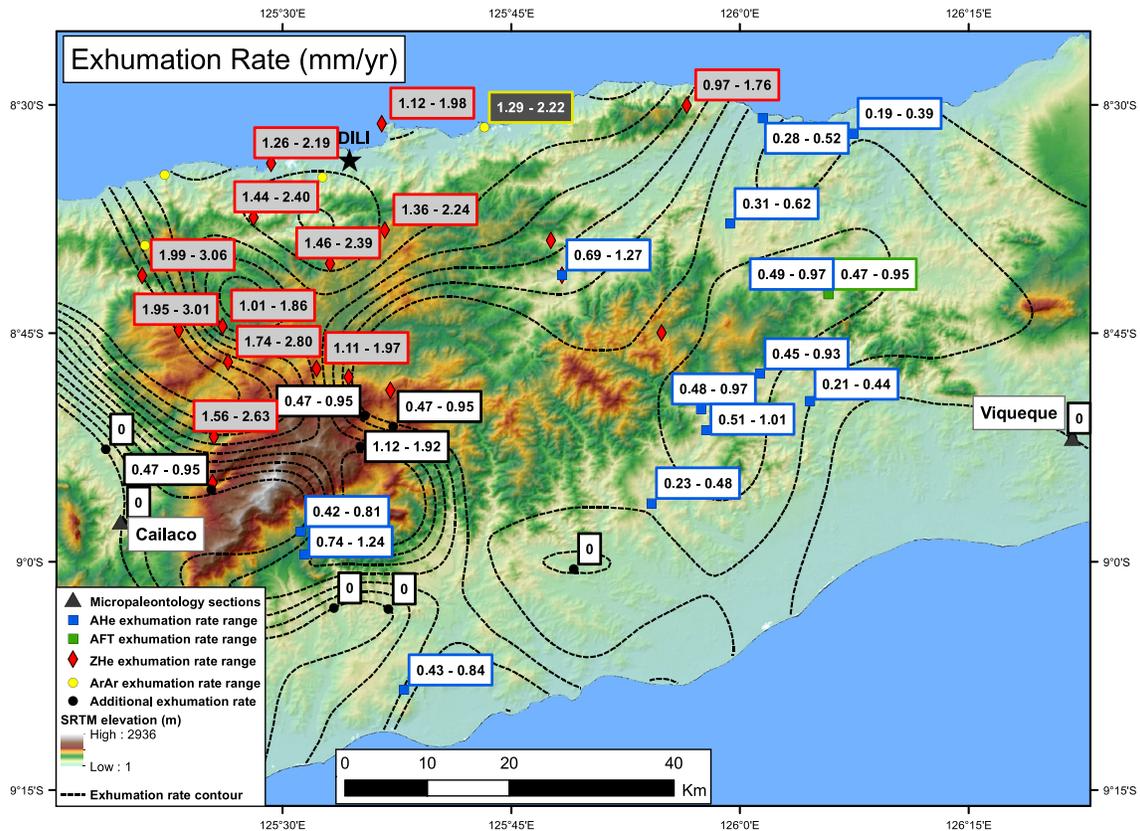
4.5. Thermal Modeling

Results from thermal modeling are included in Table S1 and are displayed in map view in Figures 6, 7, and S1.

Models of MAr exhumation rate matching a 32°C/km pre-exhumation geothermal gradient suggest exhumation rates of 1.29 mm/yr and 9.22 km of exhumation at the location of TL11-393 since the time of closure at 7.13 Ma and suggest a 62°C/km modern geothermal gradient. Models of MAr exhumation rate matching a 15°C/km pre-exhumation geothermal gradient suggest exhumation rates of 2.22 mm/yr and 15.8 km of exhumation since the time of closure at 7.13 Ma with a 43°C/km modern geothermal gradient.

ZHe exhumation rates (and modeled modern geothermal gradients) from both sets of models generally increase from east to west, whereas the modeled thickness of exhumed material generally decreases from east to west. Models reproducing a pre-exhumation geothermal gradient of 32°C/km suggest exhumation rates varying from 0.97 mm/yr in the far eastern Aileu to 1.99 mm/yr along the western edge of the slate belt, 4.3 km of exhumation in the east decreasing to as little as 2.7 km in the west and modern geothermal gradients ranging from 52°C/km in the east to 82°C/km in the west. Models reproducing a pre-exhumation geothermal gradient of 15°C/km suggest exhumation rates varying from 1.76 mm/yr in the east to 3.06 mm/yr along the western edge of the slate belt, 7.75 km of exhumation in the east decreasing to 4.47 km in the west and modern geothermal gradients ranging from 35°C/km in the east to 59°C/km in the west.

AHe exhumation rates suggested by both sets of models are generally faster at higher elevations (and correlate with average annual rainfall, see section 5.2). In the eastern map area, models reproducing a pre-exhumation geothermal gradient of 32°C/km suggest exhumation rates of 0.19–0.28 mm/yr on the north coast increasing to 0.45–0.51 mm/yr along the central mountain axis and decreasing to 0.21–0.23 mm/yr in the southern foothills. Areas farther to the west in the central mountain belt have modeled exhumation rates as high as 0.69–0.74 mm/yr, with 0.43 mm/yr modeled near the south coast in the southwest map area. Models matching

Figure 7. Range of exhumation rates in thermal modeling of thermochronology data. Rates are average exhumation rates since time of closure. The single AFT model is for an age of 5.2 Ma representing 90% of the sample grains. Contours are created from a spline of our exhumation rates (from 32°C/km initial geothermal gradient models) and additional points as shown on the map: four locations of AFT samples from *Harris et al.* [2000], and six points within synorogenic basins with no exhumation assumed (marked 0). Exhumation rates of 1.12–1.92 mm/yr are modeled from the *Harris et al.* [2000] reset age of 1.8 Ma using the same procedure from *Willett and Brandon* [2013] as the modeling results presented here. Exhumation rates of our most annealed AFT sample (with 90% of grains about 5.2 Ma) are used for the purposes of this contouring as maximum exhumation rates for three partially annealed AFT samples from *Harris et al.* [2000] with ages of 6.4 ± 4.4, 8.5 ± 5.6, and 255 ± 78 Ma.

a 15°C/km pre-exhumation geothermal gradient display a similar pattern, with exhumation rates in the east of 0.39–0.52 mm/yr on the north coast, 0.93–1.01 mm/yr in the south-central mountain belt and 0.44–0.48 mm/yr in the southern foothills and the fastest exhumation rates farther to the west in the central mountains of 1.24–1.27 mm/yr. Modeled modern geothermal gradients range from 35 to 47°C/km for the 32°C/km pre-exhumation geothermal gradient models and 18–28°C/km for the 15°C/km pre-exhumation geothermal gradient models. Modeled exhumation magnitudes are very close to 1 km in the 32°C/km pre-exhumation geothermal gradient models (ranging from 0.93 to 1.33 km) and range from 1.78 to 2.28 km in the 15°C/km pre-exhumation geothermal gradient models.

Thermal modeling was performed for the AFT age of sample TL11-61 in the eastern central mountain axis. Although this sample is not completely reset for AFT, BINOMFIT [*Brandon*, 2002] suggests that 90% of grains belong to a reset population centered about 5.2 Ma. Thermal models of this sample using 5.2 Ma as the time of closure of the apatite fission track system therefore provide a reasonable upper bound on the magnitude of exhumation in this area. Thermal-exhumation models suggest exhumation rates of 0.47–0.95 mm/yr (similar to the AHe exhumation rates for this sample), exhumation magnitudes of 2.5–4.9 km and modern geothermal gradients of 24–41°C/km.

4.6. Micropaleontology
4.6.1. Viqueque Type Section
4.6.1.1. Sedimentology
A stratigraphic column for the Viqueque type section is presented in Figure 3. The basal 12 m of the section is composed of chalky pelagic limestone that unconformably overlies the Bobonaro mélange. These carbonates

contain little to no clastic input and were deposited in a low-energy deepwater depositional environment. From 12 to 41 m, the section exposes rhythmic alternations of chalks and marls, which may represent Milankovitch-driven cyclicity, with the thickness of the cycles and the clay content increasing upward suggesting increase of sedimentation rate. From 41 m to the top of the section at 240 m, we find a succession of alternating clays, sandstones, and conglomerates [*Haig and McCartain*, 2007; *Nguyen et al.*, 2013]. This succession generally coarsens upward, with bedded sandstones and conglomerates becoming more common and clays becoming more contaminated with silt and sand upward. Individual sandstone and conglomerate beds generally fine upward, display Bouma sequences, and display scour marks and rip-up clasts at the base of the bed. The conglomerate beds are up to several meters thick and contain poorly sorted clasts of mafic rock, sandstone, and limestone clasts as well as occasional pieces of fossil wood. These are interpreted as debris flows. This trend suggests increasing proximity to the sediment source resulting from uplift and emergence of the island, as previously suggested by *Haig and McCartain* [2007] and *Nguyen et al.* [2013].

4.6.1.2. Age Control

The chalky pelagic limestone of the lowest 12 m contains planktonic foraminifers that are common but re-crystallized. Presence of *Globorotalia tumida* indicates this interval is younger than 5.59 Ma [*Lourens et al.*, 2004] or 5.57 Ma [*Wade et al.*, 2011]. The top of the chalky pelagic limestone at 12 m marks a hiatus spanning ≥ 1.22 Myr because of the simultaneous first occurrence (FO) of *Sphaeroidinella dehiscens* (dated at 5.54 Ma by *Lourens et al.* [2004] and 5.53 Ma by *Wade et al.* [2011]) and *Globorotalia crassaformis* (dated both by *Lourens et al.* [2004] and *Wade et al.* [2011] at 4.31 Ma). The interval from 12 to 17 m is characterized by calcareous marls with interbedded pelagic limestones and is bounded above by a second hiatus marked by the simultaneous disappearance of *Sphaeroidinellopsis* at 3.59 Ma [*Wade et al.*, 2011] and *Globoquadrina altispira* at 3.47 Ma [*Wade et al.*, 2011]. A few occurrences of these species are found much higher in the section at 169, 177 and 217 m, but are assumed to be reworked.

Marls dominate from 17 to 41 m, followed by clays and turbiditic sandstones to the top of the section. Occasional occurrences of *Globorotalia tosaensis* from 197 m upward indicate that the uppermost part of the section is younger than 3.35 Ma [*Wade et al.*, 2011]. Additionally, two specimens at 23 m are determined to be close to *Globorotalia tosaensis*. We favor placing the FO of *Globorotalia tosaensis* (and the corresponding 3.35 Ma marker) at 23 m instead of 197 m because *Globorotalia tosaensis* was found in a similar position near the base of the shale and turbidite sequence in the Cailaco basin and magnetostratigraphy from the same levels as our biostratigraphy in the Viqueque type section contains polarity reversals between 17 m and 197 m [*Aben et al.*, 2014], but no polarity reversals are known between 3.47 and 3.35 Ma [*Cande and Kent*, 1995; *Lourens et al.*, 2004].

Samples up to the top of the Viqueque section contain *Globigerina apertura, Globigerinoides obliquus*, and *Globigerinoides obliquus extremus*, indicating the top of the section is older than 1.98 Ma [*Lourens et al.*, 2004; *Wade et al.*, 2011]. Magnetostratigraphy in the Viqueque type section also indicates that the top of the section may be as old as 3 Ma [*Aben et al.*, 2014].

Haig and McCartain [2007] concluded that the lower 30 m of pelagic limestone and marls spans ages from about 5.6 to 3.35 Ma. These authors placed the FO of *Globorotalia tosaensis* (and the corresponding 3.35 Ma marker) at 34.4 m, a position only slightly higher than our level at 23 m.

4.6.1.3. Timing and Magnitude of Shoaling

Benthic foraminiferal faunas from the base up to 177 m are characterized by lower bathyal species (those at 2000–1000 m depth), of which *Cibicides wuellerstorfi, Oridorsalis umbonatus, Cibicides bradyi, Osangularia bengalensis, Pullenia bulloides*, and *Uvigerina hispida* have optimum depth occurrences (ODO) between 1500–2000 m [*Van Marle*, 1988, 1989]. These truly lower bathyal species are regularly associated with one or more species that have their ODO between 1500 and 1000 m, such as *Karreriella bradyi, Gyroidina orbicularis*, and *Laticarina pauperata* [*Van Marle*, 1988, 1989]. Several samples in the pelagic limestone contain 100% planktonic foraminifers indicating water depths greater than 1200 m using the regression of the *Van der Zwaan et al.* [1990] or greater than 1500 m following the regression of *Van Marle et al.* [1987].

Typically middle bathyal species (those at 1000–500 m depth) such as *Cibicides pseudoungarianus* and *Hyalinea balthica* are restricted to the interval above 163 m, but other middle bathyal species, *Uvigerina peregrina* and *Sphaeroidina bulloides*, occur already in the 37–163 m interval. All these species have their ODO between 1000 and 500 m [*Van Marle*, 1988, 1989]. The presence of *Uvigerina peregrina* and *Sphaeroidina*

bulloides in the 37–163 m interval suggests that they (slightly) overlap in depth with the truly lower bathyal species rather than being displaced from shallower depths. Occasional occurrences of the photic layer dwelling *Amphistegina* and *miliolids* above 163 m have almost certainly been transported from shallower depths.

The benthic faunas thus document a shoaling from lower bathyal (2000–1000 m) to middle bathyal (1000–500 m) depths. Perhaps, a first sign of shoaling is provided by the appearance of some middle bathyal species at ~37 m. *Haig and McCartain* [2007] placed the beginning of shoaling at about the same level, that is, at 41 m. However, our data show that the complete change-over from lower to middle bathyal faunas occurs between 163 and 177 m. This interval brackets the appearance of new middle bathyal species at 163 m and the disappearance of the lower bathyal species at 177 m. Middle bathyal conditions extend up to the top of the section.

Shoaling from lower bathyal to middle bathyal depths is therefore documented in the Viqueque type section at some time between 3.35 and 1.98 Ma. This time constraint remains constant if beginning of shoaling is placed at 37 m instead of 163–177 m. Even if FO of *Globorotalia tosaensis* is truly at 197 m instead of 23 m, uplift is no earlier than 3.47 Ma. Additionally, age constraints from magnetostratigraphy in the Viqueque type section indicate that this uplift is confined between 3.35 and ~3 Ma [*Aben et al.*, 2014]. *Haig and McCartain* [2007] used shallow water foraminifers in the lowest turbidite at 41 m to argue for island uplift, which is lower in the section than the foraminifera we find in the fine-grained deposits (less likely to have undergone significant downslope transport) suggest. We nevertheless concur with *Haig and McCartain* [2007] that uplift is first documented in the clastic part of the section sometime between 3.35 and 3 Ma, and that uplift continued after that.

4.6.2. Cailaco River Section

4.6.2.1. Sedimentology

A stratigraphic column for the Cailaco River section is presented in Figure 3. The lithological sequence of the deepwater synorogenics in the Cailaco River section is very similar to that exposed in the Viqueque type section, although along the Cailaco Section, a much thicker stratigraphy is exposed (more than 600 m of which 500 m was accessible for logging). The basal 34 m is composed of pelagic limestone and marl covering Bobonaro mélange (although the contact was not exposed), indicating a low-energy deepwater environment with little to no clastic input. An unexposed interval of 15 m separates these limestones and marls from a sequence of clays interbedded with turbiditic sandstones and conglomerates from 49 to 500 m (with several other unexposed intervals of up to several tens of meters of stratigraphy). Turbidites become more common higher in the section, and toward the top of the section, clays become rare and sandstone bodies become more massive, which may indicate some combination of shallowing and increasing proximity to the sediment source. As in the Viqueque type section, conglomerates contain clasts of mafic rock, limestone, and sandstone, consistent with unroofing of the Timor orogenic belt.

4.6.2.2. Age Control

The basal 22 m of chalky pelagic limestone and marls is dated between 5.59 and 5.53 Ma as indicated by the presence of *Globorotalia tumida* as well as the FO of *Sphaeroidinella dehiscens* at 22 m [*Lourens et al.*, 2004; *Wade et al.*, 2011]. A hiatus between 22 m and 25 m from 5.53 to 4.31 Ma is revealed by the almost simultaneous FO of *Sphaeroidinella dehiscens* at 22 m and FO of *Globorotalia crassaformis* at 25 m [*Lourens et al.*, 2004; *Wade et al.*, 2011]. Another hiatus from 3.59 to 3.47 Ma at the top of the pelagic limestones and marls at 34 m is indicated by the simultaneous disappearance of *Globoquadrina altispira* and representatives of *Sphaeroidinellopsis* [*Wade et al.*, 2011].

The FO of *Globorotalia tosaensis* is found at 94 m within the succession of clays and turbiditic sandstones and corresponds to an age of 3.35 Ma [*Wade et al.*, 2011]. Unlike the Viqueque section, *Globigerinoides fistulosis* is found in spotty occurrences at and above 113 m providing an age of 3.33 Ma for this level [*Wade et al.*, 2011]. The highest occurrence of *Globigerinoides fistulosis* is recorded at 473 m indicating that the top of the section (at 493 m) is older than 1.88 Ma [*Wade et al.*, 2011].

4.6.2.3. Timing and Magnitude of Shoaling

Lower bathyal species characterize the benthic faunas from base up to 172 m. Again, *Karreriella bradyi* and *Gyroidina orbicularis*, species with ODO between 1500 and 1000 m [*Van Marle*, 1988, 1989], co-occur with truly lower bathyal species (having their ODO between 1500 and 2000 m), such as *Cibicides wuellerstorfi*, *C. bradyi*, and *Oridorsalis umbonatus*. Percentages of planktonic foraminifers of nearly 100 in
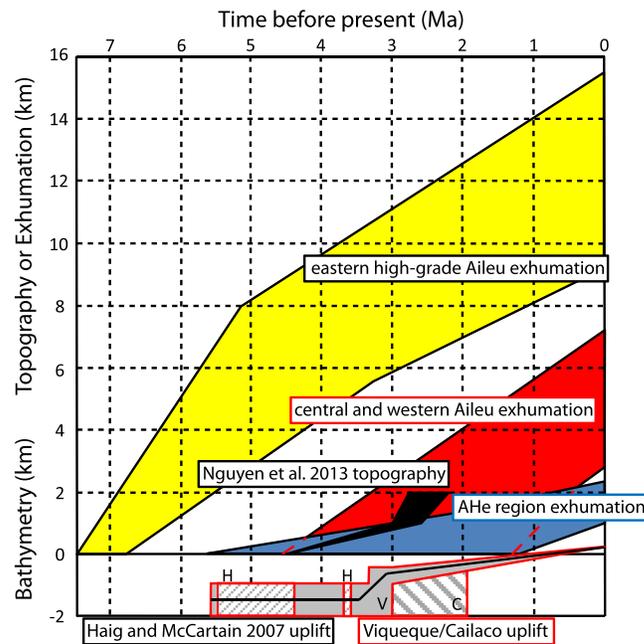
Figure 8. Exhumation and uplift of different zones through time, after Figure 4 in *Nguyen et al.* [2013]. Note the large difference in exhumation histories of different regions, as well as the significant exhumation documented within all exhuming regions both before and after a pulse of uplift in the synorogenic basins. Topography of the emergent island is included from palynology constraints of *Nguyen et al.* [2013], shown as black polygon. Timing of Viqueque type section uplift from *Haig and McCartain* [2007] is shown as black line. Exhumation histories of three zones in the central mountains are constrained by thermochronology and thermal modeling. Thermochronology age constraints take 2σ errors into account, and exhumation constraints include high and low exhumation magnitude estimates from thermal models. Possible exhumation paths of the eastern Aileu high-grade belt are constrained by thermal modeling of both MAr and ZHe data within this region and assume that these two data sets are representative of the entire region despite originating from different samples. Possible time exhumation paths of the Aileu slate belt are based on thermal modeling of ZHe data, and foreland exhumation is constrained by AHe thermal models. AFT modeling is not included, which suggests greater exhumation (up to 2.5–4.9 km) for those AHe samples in the central mountain axis. In each zone, exhumation may have proceeded earlier than indicated here and more total exhumation may have occurred, as exhumation is only constrained by samples currently preserved at the surface. Uplift histories of the Viqueque and Cailaco basins are constrained by micropaleontology. Hiatuses in the Viqueque and Cailaco sections are labeled H. Uplift by 3 Ma suggested by magnetostratigraphy by *Aben et al.* [2014] in the Viqueque section is labeled V. Later uplift permissible in Cailaco section labeled C.

the pelagic limestones and marls indicate paleodepths of ≥ 1200–1500 m [*Van der Zwaan et al.*, 1990; *Van Marle et al.*, 1987].

Typically middle bathyal species, such as *Cibicides pseudoungarianus*, *Gyroidina neosoldanii*, *Hyalinea balthica*, and representatives of *Uvigerina* and *Bolivinita* [*van Hinsbergen et al.*, 2005; *Van Marle*, 1988, 1989], are characteristic elements of the benthic faunas above 172 m. Some of these species, however, are already present between 83 and 172 m, which may indicate either some overlap in depth range with lower bathyal species or occasional downslope transport of middle bathyal species into the basin. Percentages of planktonic foraminifers from 365 to 462 m provide mean depth values of 955 ± 126 m using the regression of *van der Zwaan et al.* [1990] and 965 ± 232 m using the regression of *Van Marle et al.* [1987].

Rare occurrences of the neritic elements *Ammonia*, *miliolids*, *Elphidium*, and epiphytic *Cibicides*, which live on plants and may be subject to rafting, are recorded from 105 to 172 m. They remain present above 172 m, albeit in slightly higher numbers, consistent with the sedimentological trend of increasing proximity to land. Samples at 365 m and 456 m contain some representatives of the photic layer dwelling *Amphistegina*. All these neritic elements are considered to be transported by turbidity flows from shallower depths or by rafting.

The benthic faunas in the Cailaco River section thus document shoaling from lower (2000–1000 m) to middle bathyal (1000–500 m) depths around 172 m, i.e., sometime between 3.33 and 1.88 Ma. Perhaps, a first sign of shoaling is provided by the appearance of middle bathyal species at 83 m. Middle bathyal conditions extend up to the top of section. Both the magnitude and the timing of shoaling in the Cailaco River section are consistent with that recorded for the Viqueque type section.

5. Discussion

5.1. Temporal History of Uplift and Exhumation

Figure 8 summarizes the evolution of exhumation and surface uplift for four distinct zones within our data sets: the eastern Aileu high-grade belt, the Aileu slate belt, the Gondwana Sequence regions containing AHe data, and the Viqueque and Cailaco synorogenic basins. MAr models indicate that the eastern Aileu high-grade belt

has exhumed 9.2–15.8 km since 7.1 ± 0.3 Ma, and exhumation rates appear to have been faster before ZHe closure than after because modeled ZHe exhumation rates in this area are slower than modeled MAr exhumation rates. Sample localities across the Aileu slate belt have exhumed 2.7–7.1 km since 4.5–1.3 Ma. While exhumation rates are similar in the Aileu high-grade and Aileu slate belts, exhumation has proceeded for a longer time in the Aileu high-grade belt. AHe localities have exhumed 0.9–2.3 km since 5.6–1.2 Ma, with exhumation magnitudes up to 2.5–4.9 km since 5.2 Ma in locations where we find the greatest degree of annealing in AFT. The Viqueque and Cailaco basins have uplifted from 1–2 km depths to 350–1000 m depths sometime between 3.35 and 1.88 Ma, and after deposition of their youngest sediments, the two sections have uplifted to present-day elevations of 50 and 300 m, respectively. Although these zones are each dominated by data sets with very different closure temperatures (62–74°C for AHe, 116–118°C for AFT, 188–207°C for ZHe, and 279–349°C for MAr according to our simulations), at the edge of each zone, samples with multiple thermochronometers allow us to compare the total amount of exhumation between each zone. For example, seven AHe samples are shown to have old AFT populations that were not fully annealed and our youngest AHe sample is shown to have unreset ZHe, limiting total exhumation in the region of AHe samples. Also, our unreset ZHe samples at the southern edge of the Aileu slate belt are in the same area as partially annealed AFT from *Harris et al.* [2000], limiting total exhumation there even further. Additionally, several of the youngest ZHe samples are near to unreset MAr ages, limiting total exhumation in the western Aileu slate and high-grade belts.

The thermochronology data provide constraints on the timing and spatial extent of earliest emergence on Timor. *Nguyen et al.* [2013] argue that earliest emergence occurred just before 4.45 Ma as indicated by an increase in clastic input in the Viqueque type section as well as an increase in pollen types that are characteristic of lowland rainforests and mangrove swamps. In the eastern map area, AHe samples from both the north coast and southern foothills are within error of 4.45 Ma, and it is likely that the central eastern map area began exhuming ~5 Ma as well based on modeling of AFT ages. Young AHe ages of ~2 Ma in this area are the result of continuing, fast exhumation eliminating the earliest signal of exhumation within this system. Several ZHe ages are also within error of 4.45 Ma in the eastern Aileu high-grade belt and at one location in the central Aileu slate belt. Because this widespread signal of exhumation in our thermochronology data is coincident with independent constraints of island emergence, we suggest that a wide area of Timor was emergent at ~4.5 Ma. This area would have minimally included the locations of the present-day surface exposure of the eastern Aileu high-grade belt and the Gondwana Sequence in the eastern map area, as well as a region north of the Viqueque type section (as constrained by paleocurrent measurements in the Viqueque type section [*Nguyen et al.*, 2013]). The western Aileu high-grade belt, the Aileu slate belt, and the western Gondwana Sequence along the central mountain axis may have been emergent at 4.5 Ma as well, but our thermochronology data do not constrain this because most of the ages are younger than 4.5 Ma. Despite the close proximity (15 km) of these areas to the Pliocene sediments of the Cailaco River section, the western Aileu slate belt and the high peaks of western Gondwana Sequence could have been emergent while the Cailaco basin was at lower bathyal depths if the topographic gradient was similar to the modern gradient. Emergence of the western Aileu slate belt as early as 4.5 Ma is permitted by the stratigraphy of the Cailaco basin, as marls are interbedded with the pelagic limestones at this time. Alternatively, the western slate belt may not have emerged until ~3.5 Ma, which is within error of the oldest reset ZHe ages in the slate belt and also the age of the start of interbedded marl and turbidite deposition at Cailaco. Early emergence of such a wide area of Timor is contrary to previous interpretations of synorogenic basin data, such as *Audley-Charles* [2004] who argues that the entirety of Timor was several kilometers deep at 5 Ma or *Haig* [2012] who argues that at most the Aileu high-grade belt was emergent at ~4.5 Ma.

Additionally, the thermochronology presented here suggests that exhumation initiated earlier than all previous estimates of Timor island emergence. A MAr age of 7.1 Ma and an AHe age of 5.5 Ma from rocks presently exposed on the northern coast of Timor require that initiation of exhumation in those areas began significantly earlier than 4.45 Ma. Although the earliest sample of *Nguyen et al.* [2013] that contains significant pollen contributions from lowland rainforests and mangrove swamps is at 4.45 Ma, only a single palynology sample constrains pre-4.45 Ma pollen sources and their data set displays a large variability in the relative contribution of pollen types, allowing the possibility that part of Timor was emergent before 4.45 Ma. In addition, an emergent landmass in the eastern Aileu high-grade belt may have been too distal to provide significant clastic input to the Viqueque section (the two locales are presently 80 km apart and may have been hundreds of kilometers apart at 7.1 Ma depending upon estimates of crustal shortening [*Harris*, 1991;

Tate et al., 2010]). Alternatively, exhumation in the eastern Aileu high-grade belt without emergence at 7.1 Ma would imply significant submarine exhumation (3.5–9 km before 4.45 Ma; see Figure 8) in the hinterland of the orogen. Submarine exhumation in some areas of Timor is in fact suggested by the absence of the Banda Terrane and the Kolbano Sequence below the basal deepwater Viqueque Sequence at our two studied sections, discussed in more detail in section 5.3.

Despite the possibility that wide areas of the central mountain belt were emergent at ~4.5 Ma, locales preserving deepwater synorogenics were submarine at this time and foraminiferal records do not demonstrate uplift until much later. Our micropaleontology data from the Viqueque and Cailaco sections suggest uplift from lower bathyal to upper-middle bathyal depths sometime between 3.35 and 1.88 Ma. Depth estimates using paleobathymetry calibrations of *Van Marle* [1988, 1989, 1991] indicate uplift from depths of 1500–2120 m to 600–1000 m and a minimum uplift rate of 0.34 mm/yr, and calibrations from *van Hinsbergen et al.* [2005] indicate uplift from depths greater than 1000 m to 350–600 m depth and a minimum uplift rate of 0.27 mm/yr. Restriction of uplift to 3.35–3.0 Ma, as suggested by *Aben et al.* [2014], would indicate minimum uplift rates of 1.43 mm/yr with the depth estimates of *Van Marle* [1988, 1989, 1991] or 1.14 mm/yr with the depth estimates of *van Hinsbergen et al.* [2005]. (As the only age constraints are before and after the shift from lower bathyal to upper-middle bathyal foraminifera, the maximum uplift rate is unconstrained.) The timing of uplift of *Haig and McCartain* [2007] (also shown in Figure 8) is within the timing constraints provided by our data set. Although foraminifera within the Viqueque and Cailaco sections provide roughly equivalent age and paleodepth constraints, the errors associated with these data allow for the possibility that the two basins experienced uplift from lower bathyal to upper-middle bathyal depths up to 1.5 Myr apart.

Overall, the four zones of the Aileu high-grade belt, the Aileu slate belt, the foreland exposures of the Gondwana Sequence, and the synorogenic basins show distinctly different exhumation and uplift paths through time. Exhumation started significantly earlier in the northern Aileu high-grade belt than in other more southerly zones. Although much more exhumation has occurred in the Aileu slate belt than the southern and eastern Gondwana Sequence exposures, the eastern Gondwana Sequence exposures were likely among the earliest emergent areas of the island. Our data also suggest that both the Viqueque and Cailaco sections were still at lower bathyal depths while wide areas of Timor were emergent and exhuming at ~4.5 Ma and that significant exhumation had proceeded throughout the central mountain belt before these two synorogenic sections experienced demonstrable uplift. The synchroneity of these deep synorogenic basins and exhumed mountain belts leads to some of the most striking examples of the spatial heterogeneity of uplift and exhumation noted below.

5.2. Spatial Heterogeneity of Uplift and Exhumation

Estimates of total surface uplift during orogenesis show large variation over very narrow length scales on Timor. Following a phase of rapid uplift from lower bathyal to upper-middle bathyal depth sometime between 3.35 and 1.88 Ma, the deepwater synorogenic sections have been uplifted to their present elevations of 50 m in Viqueque and 300 m in Cailaco. Using estimates of lower bathyal depths suggested by *Van Marle* [1988, 1989, 1991] and *van Hinsbergen et al.* [2005], our data suggest total surface uplift of 1–2.1 km at the Viqueque section and 1.3–2.4 km at the Cailaco section to present-day elevations. For lack of constraints on the paleobathymetry of the paleosurface of other, now-exhumed areas of Timor, we consider the paleodepth of the basal Viqueque Sequence as our best estimate of depth before orogenesis and uplift of these regions as well. We would therefore suggest that locations sampled for thermochronology have experienced surface uplift from at least lower bathyal depths (possibly more, considering the modern deformation front is at ~3 km depth) to their present elevations. For areas evaluated for AHe and AFT thermochronology, this is equivalent to a minimum of 1–2 km of uplift (using *van Hinsbergen et al.* [2005] depths and varying elevation for each sample) or a maximum of 2.1–3.1 km (using *Van Marle* [1988, 1989, 1991] depths). Similarly, locations sampled for ZHe have experienced a minimum of 1–2.5 km of surface uplift or a maximum of 2.1–3.6 km. The current peak of the Timor mountain range, 20 km east of the Cailaco section, has experienced 4.0 to 5.1 km of surface uplift.

Records of exhumation, however, demonstrate an even higher degree of spatial variability on the island. Locations sampled for the Viqueque Sequence appear to have experienced at most a few hundred meters of exhumation, as only a presumably thin upper synorogenic cover has been removed. Not far from these locations, however, thermal modeling suggests several kilometers of exhumation. Areas evaluated for AHe
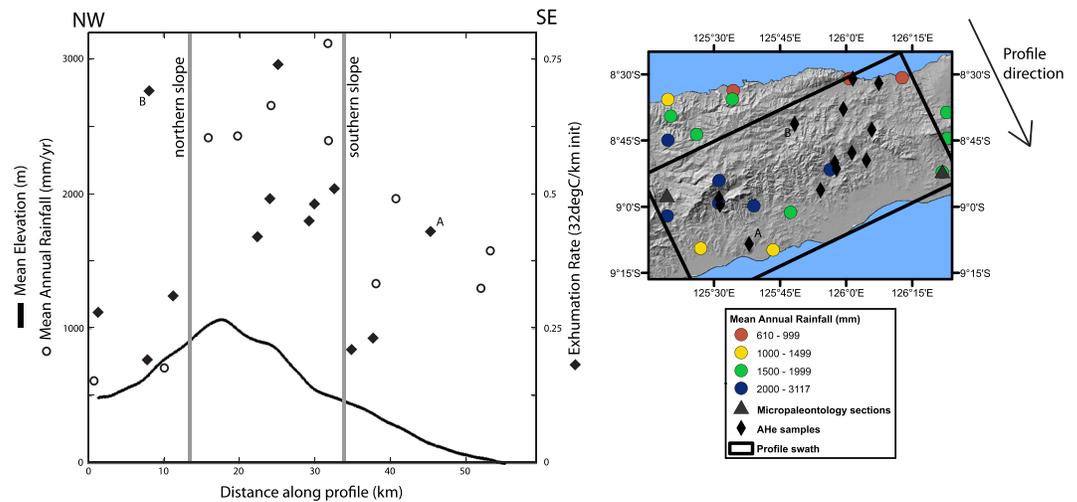
Figure 9. NW-SE profile of mean elevation, mean annual precipitation and modeled AHe exhumation rate. Sharp gradients in precipitation and exhumation rate are highlighted along the denoted northern and southern slopes. Map of average annual rainfall and profile swath shown to right. Rainfall data from *Timor-Leste Ministry of Agriculture* [2012]. Samples with anomalously high exhumation rates are labeled A and B. A corresponds to the greater degree of exhumation on the SW coast compared to the SE coast. B, despite its location near the north end of the profile, is within the more quickly exhuming interior of the island.

have experienced 0.9–2.3 km of exhumation since the time of AHe closure depending on estimates of the starting geothermal gradient. Areas along the central mountain axis have experienced greater total exhumation than this, as thermal modeling of nearly completely reset apatite fission track populations suggests up to 2.5–4.9 km of exhumation. Thermal models of ZHe data in the central Aileu belt suggest 3.3–7.1 km of exhumation since the time of closure, depending on the initial geothermal gradient. Along the western edge of high topography of the Aileu slate belt, thermal models suggest 2.7–4.8 km of exhumation since ZHe closure. This relatively lower amount of exhumation compared to the central Aileu belt is due to the high modeled geothermal gradient resulting from the fast exhumation implied by ZHe ages of less than 2 Ma. One of these western Aileu samples is 15 km from the Cailaco synorogenic section, demonstrating one of the largest gradients in exhumation on Timor. The eastern Aileu high-grade belt, where MAr ages are reset, is modeled to have experienced 9.2 to 15.8 km of exhumation. Total amounts of exhumation in all locations may have been greater than the estimates provided from the thermal models, as exhumation is likely to have proceeded before the time recorded by the thermochronology samples preserved at the surface.

Even within the zone of lower total magnitudes of exhumation recorded by AHe data, there is still significant variability in age and exhumation rate. Figure 9 (where average elevation, average annual precipitation, and exhumation rate from a 120 km wide swath are plotted along a northwest-southeast profile perpendicular to the structural trend of the island) demonstrates a correlation between AHe exhumation rate and mean annual rainfall along the southern mountain slopes. AHe exhumation rate is approximately twice as fast and average annual rainfall is approximately twice as large along the central mountain axis as in the southern foothills and in the foothills of the northeast map area. The transition between these zones of exhumation rate is strikingly narrow, constrained to be less than 5 km wide along the southern slopes. High AHe exhumation rates are not symmetrically distributed about the highest topography, but rather they most closely follow patterns of average annual rainfall that are highest on the southern side of the mountain axis. This stronger correlation of exhumation rate with average annual rainfall rather than with elevation suggests that rainfall may play a key part in determining the modern patterns of exhumation on Timor.

The transition from reset to unreset ZHe ages is very near to the southern boundary of the Aileu slate belt. Apatite fission track data presented by *Harris et al.* [2000] near several of our unreset ZHe samples suggest a thermal history in the Gondwana Sequence just south of the Aileu slate belt that reaches temperatures only high enough to partially anneal apatite fission tracks. Furthermore, vitrinite reflectance data presented by *Harris et al.* [2000] are between 1.0 and 2.4 south of the slate belt, yet abruptly increase to 3.3 north of the slate belt boundary near our sample TL11-217 which has a ZHe age of 3.6 ± 0.9 Ma. These data suggest a very

steep gradient in peak temperature between our reset and unreset ZHe samples and support the interpretation that there is a large gradient in total exhumation close to the boundary between the Aileu slate belt and the Gondwana Sequence in our western map area.

Both surface uplift and exhumation therefore demonstrate wide variability across the island. This variability is striking both in the range of absolute magnitudes and the narrow transition zones along which differential uplift and exhumation are accommodated. Magnitudes of exhumation are for the most part broadly consistent within the interior of each of the foreland, slate, and high-grade zones. Steep boundaries in exhumation are documented on the flanks of the exposures of the Gondwana Sequence, at the boundary between the Gondwana Sequence and the Aileu slate belt, and at the juxtaposition of the synorogenic basins with the Aileu Complex and Gondwana Sequence. Any unified driving process proposed to cause this heterogeneity in exhumation must account for both the broad extent of and sharp boundaries between the distinct zones of exhumation we observe.

5.3. Processes Driving Variable Uplift and Exhumation

The correlation between AHe exhumation and average annual rainfall rates and the shifted position of the peak rates relative to the topographic form of the range are consistent with a dynamic feedback between precipitation, erosion, and rock uplift [*Reiners et al.*, 2003; *Willett*, 1999]. Modeled exhumation rates double from the southern foothills to the south-central range over a distance of less than 5 km. The small length scale of the variability in exhumation rate requires a shallow depth ≤ 5 km for the controlling mechanism. Surface faulting is one mechanism that could cause such a sharp gradient in exhumation, but preliminary structural mapping demonstrates that surface faults of the Gondwana Sequence duplex are not currently active because they have been folded since the time that they were active thrusts [*Tate et al.*, 2010] and because no thrust faults within the Gondwana Sequence duplex are observed to cut the overriding Banda klippen [*Harris*, 2006; *Harris et al.*, 1998; *Standley and Harris*, 2009; *Tate et al.*, 2010]. In addition, this transition from the southern foothills to the south-central range in the eastern map area does not correlate with any of the proposed normal faults on the island [*Duffy et al.*, 2013]. Fault propagation folding due to a blind thrust in the subsurface could explain the sharp boundary in exhumation rates at the southern range front, but a single blind thrust would not explain the wide extent of fast exhumation rates continuing toward the hinterland in the northwest. A third possible mechanism driving differential exhumation is subsurface duplexing. *Harris* [1991] and *Zobell* [2007] observed repeating lithologies best explained by duplexing of the Gondwana Sequence in Timor-Leste, and mapped thrust faults within the Gondwana Sequence in Figure 1 show portions of this duplex now exposed at the surface. Although the thrust faults of the duplex exposed at the surface are not currently active, it would be reasonable to expect similar geometries of faulting to be active today. Broad culminations of subsurface duplexes are consistent with the general pattern of Gondwana Sequence antiforms and Banda Terrane synforms across the island [*Harris et al.*, 2000] and provide a mechanism to produce a broad uplift pattern consistent with the observed wide swath of fast exhumation rates. Subsurface thrust ramps may also control part of the structural deformation of the region, and could have played a role in exhuming the portion of the duplex now exposed at the surface.

One of the largest gradients in exhumation we observe is the gradient along the western edge of the Aileu Complex. Here ZHe data suggest exhumation of 2.7–4.6 km since 1.8 Ma only 15 km away from the Cailaco basin that has likely experienced less than a few hundred meters of exhumation. A normal fault located at the edge of the Cailaco River valley that juxtaposes the Aileu Complex with the Viqueque Sequence and Bobonaro Mélange accommodates much of the observed differential surface uplift between these two regions [*Duffy et al.*, 2013]. If this normal fault were driven by an island-scale extensional tectonic setting on Timor, one would expect significant subsidence of the hanging wall and an alluvial sedimentary package within the hanging wall that is several kilometers thick. On the contrary, we note that both the footwall of Aileu Complex and hanging wall of Viqueque Sequence and Bobonaro Mélange have experienced significant uplift to their present elevations since 3.35 Ma, and the Cailaco River valley does not have a significant alluvial sedimentary package. This suggests that this normal fault is not driven by a large-scale extensional tectonic setting, but may be a more passive response to subsurface duplexing. Duplexing below both the footwall and hanging wall would cause uplift of both fault blocks, and a greater degree of duplexing below the Aileu Complex would cause more uplift of the footwall. *Duffy et al.* [2013] have argued that duplexing below the footwall initiated motion along the Marobo fault, and our data suggest this duplexing continues today. Duplexing below the Aileu Complex is also consistent with the interpretation that a significant boundary in

exhumation exists near the southern boundary of the Aileu slate belt. A large young duplex culmination below the slate belt, coupled with out-of-sequence thrusting near the southern limit of the slate belt, would explain the sharp gradient in exhumation magnitude observed across this boundary.

The Viqueque and Cailaco basins, as well as other basins where the Viqueque Sequence is present, are positioned along the margins of the broad plunging antiforms mapped across Timor [*Harris et al.*, 2000]. In all of these locations, the Viqueque Sequence is deposited unconformably on the Bobonaro Mélange. As discussed above in section 2, both the Banda Terrane and the Kolbano Sequence are absent between the Viqueque Sequence and the Bobonaro Mélange at our studied sections. We propose that as topography developed from duplexing of the Gondwana Sequence and Aileu Complex, gravitational sliding along the weak Bobonaro Mélange caused slumping and local normal faulting along the plunging margins of the duplex. In the case of the foreland Viqueque basin along Timor-Leste's south coast and in the Central Basin of West Timor, this gravitational sliding translated the Kolbano Sequence fold-thrust belt to the south, while in the hinterland Cailaco basin this gravitational sliding removed the Banda Terrane. As the basal pelagic limestones of the Viqueque Sequence are dated at 5.59 to 5.53 Ma, this interpretation would suggest that significant submarine topography had developed by this time. A similar process south of the island of Savu has been suggested by *Harris* [1991, 2011], where the foreland wedge of structurally repeated Kolbano Sequence has undergone collapse.

Submarine unroofing provides an intriguing option for explaining exhumation from 7.1 to 4.5 Ma, as palynology, micropaleontology, and sedimentology in the Viqueque basin have been interpreted to indicate earliest island emergence close to 4.45 Ma [*Nguyen et al.*, 2013]. The consistent absence of the Banda Terrane and the Kolbano Sequence between the Viqueque Sequence and the Bobonaro Mélange provides direct evidence that significant submarine exhumation has occurred at Timor. It is possible that some component of early exhumation in the Aileu high-grade belt was not driven by erosion linked to emergence above sea level, but rather by submarine gravitational sliding of the Banda Terrane lid along the weak Bobonaro Mélange décollement resulting from oversteepening of the northern margins of the orogen. Oversteepening was likely the result of subsurface duplexing below the Aileu Complex.

The mechanisms driving patterns of differential exhumation have implications for the current tectonic regime on Timor. Authors have reported conflicting models for the nature of the downgoing slab at Timor. Although some have invoked slab tear at the ocean-continent transition to explain a gap in observed seismicity [*Ely and Sandiford*, 2010; *Mccaffrey et al.*, 1985; *Sandiford*, 2008], others argue that tomography suggests a continuous subducting slab [*Fichtner et al.*, 2010; *Spakman and Hall*, 2010]. Some previous structural interpretations suggest active tectonics is dominated by large-scale extension and invoke rebound resulting from slab breakoff as the driving cause [*Charlton*, 1991; *Keep and Haig*, 2010]. Uplift of the Viqueque basin since 3.35 Ma has been interpreted to be the result of ~2 km of regional uplift due to isostatic rebound [*Keep and Haig*, 2010]. One would expect several kilometers of regional uplift to be manifest as increased exhumation rates since 3.35 Ma in our thermochronology data set, but no such regional acceleration of exhumation is found. Moreover, if the arguments in section 5.1 hold and the entire eastern map area with AHe ages was emergent at 4.5 Ma, any sample location currently near sea level would have experienced magnitudes of exhumation equal to any signal of uplift since 4.5 Ma. If isostatic rebound caused 2 km of uplift across Timor since 3.35 Ma, low-elevation AHe samples that began exhuming before 3.35 Ma would have experienced 2 km of additional exhumation since this time, completely resetting any AHe age older than 3.35 Ma. As samples along the north coast and in the low-elevation southern foothills give AHe ages of 4.5 Ma and older, we do not consider it likely that Timor has experienced an island-scale uplift signal of significant magnitude that is concurrent with the uplift signal in the Viqueque basin. Also, Banda forearc rocks mapped at the surface of Timor have been interpreted by some as Australian basement and used to argue for large-scale extension [*Charlton*, 2002]. However, U/Pb analyses of these units yield ages of 87 Ma [*Standley and Harris*, 2009] and 35 Ma [*Harris*, 2006], indicating that they originated from the overriding Banda Arc, thus limiting the magnitude of extension. Although we agree that there are extensional features that exert significant control on the modern topography, we argue that these features, like the juxtaposition of the western Aileu slate belt with the Cailaco basin, are not indicative of an island-scale extensional regime. Any subsurface basement-involved deformation or lithosphere-scale uplift mechanism would cause gradients in exhumation with wavelengths greater than the 5 km we observe. The observations presented here are best explained by active shallow subsurface duplexing. This would support the interpretation that Timor is an actively shortening orogenic wedge driven by active subduction of the Australian plate in the present day.

6. Conclusions

New thermochronology and micropaleontology data sets reveal a history of uplift in Timor-Leste that is highly heterogeneous over different spatial scales. Over a few tens of kilometers, deepwater synorogenic basins recording up to 1–2.4 km of surface uplift and little to no exhumation are juxtaposed with areas exhibiting AHe and partially reset AFT ages recording 0.9–4.9 km of exhumation, areas exhibiting ZHe ages recording 2.7–7.8 km of exhumation, and areas with reset MAr ages documenting 9.2–15.8 km of exhumation. All of this differential uplift has occurred since the late Miocene, and the fortuitous preservation of these varied signals is likely related to Timor's status as one of the world's youngest orogens. This allows us a unique window into the earliest stages of orogenic processes and an opportunity to document the maximum possible spatial variations in uplift in convergent orogens.

These data additionally provide important constraints on the style of structural development of Timor. Rapid rates of exhumation appear to be driven by subsurface duplexing below both the Aileu Complex and exposures of the Gondwana Sequence at a depth of about 5 km. Duplexing in the eastern map area in particular appears to be associated with surface erosion, correlated with average annual rainfall. Active subsurface duplexing implies underplating of Australian continental material in the present day and suggests subduction of corresponding Australian lower crust, which has implications for regional tectonic models and seismic hazard assessments in Timor-Leste.

References

Aben, F. M., M. J. Dekkers, R. R. Bakker, D. J. J. van Hinsbergen, W. J. Zachariasse, G. W. Tate, N. McQuarrie, R. Harris, and B. Duffy (2014), Untangling inconsistent magnetic polarity records through an integrated rock magnetic analysis: A case study on Neogene sections in East Timor, *Geochem. Geophys. Geosyst.*, doi:10.1002/2014GC005294.

Audley-Charles, M. G. (1968), The geology of Portuguese Timor, *Geol. Soc. London Mem.*, *4*, 84.

Audley-Charles, M. G. (2004), Ocean trench blocked and obliterated by Banda forearc collision with Australian proximal continental slope, *Tectonophysics*, *389*(1–2), 65–79.

Audley-Charles, M. G. (2011), Tectonic post-collision processes in Timor, in *The SE Asian Gateway: History and Tectonics of the Australia-Asia Collision*, edited by R. Hall, M. A. Cottam, and M. E. Wilson, *Geol. Soc. London Spec. Publ.*, *355*, 241–266.

Benincasa, A., M. Keep, and D. W. Haig (2012), A restraining bend in a young collisional margin: Mount Mundo Perdido, East Timor, *Aust. J. Earth Sci.*, *59*(6), 859–876.

Berry, R. F., and A. E. Grady (1981), Deformation and metamorphism of the Aileu formation, north coast, East Timor and its tectonic significance, *J. Struct. Geol.*, *3*(2), 143–167.

Berry, R. F., and I. McDougall (1986), Interpretation of Ar-40/Ar-39 and K/Ar dating evidence from the Aileu formation, East-Timor, Indonesia, *Chem. Geol.*, *59*(1), 43–58.

Bird, P. R., and S. E. Cook (1991), Permo-Triassic successions of the Kekneno area, West Timor: Implications for paleogeography and basin evolution, *J. Southeast Asian Earth Sci.*, *6*, 359–371.

Brandon, M. T. (2002), Decomposition of mixed grain age distributions using BINOMFIT, *On Track*, *24*, 13–18.

Cande, S. C., and D. V. Kent (1995), Revised calibration of the geomagnetic polarity timescale for the late Cretaceous and Cenozoic, *J. Geophys. Res.*, *100*(B4), 6093–6095, doi:10.1029/94JB03098.

Carter, D. J., M. G. Audley-Charles, and A. J. Barber (1976), Stratigraphical analysis of island arc-continental margin collision in eastern Indonesia, *J. Geol. Soc. London*, *132*, 179–198.

Charlton, T. R. (1991), Postcollision extension in arc-continent collision zones, eastern Indonesia, *Geology*, *19*(1), 28–31.

Charlton, T. R. (2002), The structural setting and tectonic significance of the Lolotoi, Laclubar and Aileu metamorphic massifs, East Timor, *J. Asian Earth Sci.*, *20*(7), 851–865.

Charlton, T. R., A. J. Barber, and S. T. Barkham (1991), The structural evolution of the Timor collision complex, eastern Indonesia, *J. Struct. Geol.*, *13*(5), 489–500.

Cox, N. L. (2009), Variable uplift from quaternary folding along the northern coast of East Timor, based on U-series age determinations of coral terraces, 151 pp., Brigham Young University.

DeCelles, P. G., M. N. Ducea, P. Kapp, and G. Zandt (2009), Cyclicity in Cordilleran orogenic systems, *Nat. Geosci.*, *2*(4), 251–257.

Desmet, M. E. M., A. R. Fortuin, S. R. Troelstra, L. J. Vanmarle, M. Karmini, S. Tjokosaproetro, and S. Hadiwasastra (1990), Detection of collision-related vertical movements in the Outer Banda Arc (Timor, Indonesia), using micropaleontological data, *J. Southeas Asian Earth Sci.*, *4*(4), 337–356.

Donelick, R. A., P. B. O'Sullivan, and R. A. Ketcham (2005), Apatite fission-track analysis, *Rev. Miner. Geochem.*, *58*, 49–94.

Duffy, B., M. Quigley, R. Harris, and U. Ring (2013), Arc-parallel extrusion of the Timor sector of the Banda arc-continent collision, *Tectonics*, *32*, 641–660, doi:10.1002/tect.20048.

Elburg, M. A., M. J. van Bergen, and J. D. Foden (2004), Subducted upper and lower continental crust contributes to magmatism in the collision sector of the Sunda-Banda arc, Indonesia, *Geology*, *32*(1), 41–44.

Ely, K. S., and M. Sandiford (2010), Seismic response to slab rupture and variation in lithospheric structure beneath the Savu Sea, Indonesia, *Tectonophysics*, *483*(1–2), 112–124.

Ely, K. S., M. Sandiford, M. L. Hawke, D. Phillips, M. Quigley, and J. E. dos Reis (2011), Evolution of Atauro Island: Temporal constraints on subduction processes beneath the Wetar zone, Banda Arc, *J. Asian Earth Sci.*, *41*(6), 477–493.

Ely, K. S., M. Sandiford, D. Phillips, and S. D. Boger (2014), Detrital zircon U-Pb and 40Ar/39Ar hornblende ages from the Aileu Complex, Timor-Leste: Provenance and metamorphic cooling history, *J. Geol. Soc. London*, *171*(2), 299–309, doi:10.1144/jgs2012-065.

Farley, K. A. (2002), (U-Th)/He dating: Techniques, calibrations, and applications, *Noble Gases Geochem. Cosmochem.*, *47*, 819–844.

Fichtner, A., M. De Wit, and M. van Bergen (2010), Subduction of continental lithosphere in the Banda Sea region: Combining evidence from full waveform tomography and isotope ratios, *Earth Planet. Sci. Lett.*, *297*(3–4), 405–412.

Fitzgerald, P. G., R. B. Sorkhabi, T. F. Redfield, and E. Stump (1995), Uplift and denudation of the central Alaska range - A case-study in the use of apatite fission-track thermochronology to determine absolute uplift parameters, *J. Geophys. Res.*, *100*(B10), 20,175–20,191, doi:10.1029/95JB02150.

Flowers, R. M., B. P. Wernicke, and K. A. Farley (2008), Unroofing, incision, and uplift history of the southwestern Colorado Plateau from apatite (U-Th)/He thermochronometry, *Geol. Soc. Am. Bull.*, *120*(5–6), 571–587.

Ganerød, M., D. M. Chew, M. A. Smethurst, V. R. Troll, F. Corfu, F. Meade, and T. Prestvik (2011), Geochronology of the Tardree Rhyolite Complex, Northern Ireland: Implications for zircon fission track studies, the North Atlantic Igneous Province and the age of the Fish Canyon sanidine standard, *Chem. Geol.*, *286*(3–4), 222–228.

Garzione, C. N., P. Molnar, J. C. Libarkin, and B. J. MacFadden (2006), Rapid late Miocene rise of the Bolivian Altiplano: Evidence for removal of mantle lithosphere, *Earth Planet. Sci. Lett.*, *241*(3–4), 543–556.

Garzione, C. N., G. D. Hoke, J. C. Libarkin, S. Withers, B. MacFadden, J. Eiler, P. Ghosh, and A. Mulch (2008), Rise of the Andes, *Science*, *320*(5881), 1304–1307.

Haig, D. W. (2012), Palaeobathymetric gradients across Timor during 5.7–3.3 Ma (latest Miocene-Pliocene) and implications for collision uplift, *Palaeogeogr. Palaeoclimatol. Palaeoecol.*, *331*, 50–59.

Haig, D. W., and E. McCartain (2007), Carbonate pelagites in the post-Gondwana succession (Cretaceous-Neogene) of East Timor, *Aust. J. Earth Sci.*, *54*(6), 875–897.

Hames, W. E., and S. A. Bowring (1994), An empirical-evaluation of the argon diffusion geometry in muscovite, *Earth Planet. Sci. Lett.*, *124*(1–4), 161–167.

Harris, R. (1991), Temporal distribution of strain in the active Banda orogen: A reconciliation of rival hypotheses, *J. Southeast Asia Earth Sci.*, *6*, 373–386.

Harris, R. (2006), Rise and fall of the Eastern Great Indonesian arc recorded by the assembly, dispersion and accretion of the Banda Terrane, Timor, *Gondwana Res.*, *10*(3–4), 207–231.

Harris, R. (2011), The nature of the Banda Arc-continent collision in the Timor region, in *Arc-Continent Collision*, edited by D. Brown and P. D. Ryan, pp. 163–211, Springer Heidelberg, Berlin.

Harris, R., and T. Long (2000), The Timor ophiolite, Indonesia: Model or myth?, *Geol. Soc. Am. Spec. Pap.*, *349*, 321–330.

Harris, R., R. K. Sawyer, and M. G. Audley-Charles (1998), Collisional melange development: Geologic associations of active melange-forming processes with exhumed melange facies in the western Banda orogen, Indonesia, *Tectonics*, *17*(3), 458–479, doi:10.1029/97TC03083.

Harris, R., J. Kaiser, A. Hurford, and A. Carter (2000), Thermal history of Australian passive margin cover sequences accreted to Timor during Late Neogene arc-continent collision, Indonesia, *J. Asian Earth Sci.*, *18*(1), 47–69.

Harris, R., M. W. Vorkink, C. Prasetyadi, E. Zobell, N. Roosmawati, and M. Apthorpe (2009), Transition from subduction to arc-continent collision: Geologic and neotectonic evolution of Savu Island, Indonesia, *Geosphere*, *5*(3), 152–171.

Hilton, D. R., and H. Craig (1989), A helium isotope transect along the Indonesian archipelago, *Nature*, *342*(6252), 906–908.

Hurford, A. J., and P. F. Green (1983), The zeta-age calibration of fission-track dating, *Isot. Geosci.*, *1*(4), 285–317.

Kaneko, Y., S. Maruyama, A. Kadarusman, T. Ota, M. Ishikawa, T. Tsujimori, A. Ishikawa, and K. Okamoto (2007), On-going orogeny in the outer-arc of the Timor-Tanimbar region, eastern Indonesia, *Gondwana Res.*, *11*(1–2), 218–233.

Karig, D. E., A. J. Barber, T. R. Charlton, S. Klemperer, and D. M. Hussong (1987), Nature and distribution of deformation across the Banda Arc Australian collision zone at Timor, *Geol. Soc. Am. Bull.*, *98*(1), 18–32.

Keep, M., and D. W. Haig (2010), Deformation and exhumation in Timor: Distinct stages of a young orogeny, *Tectonophysics*, *483*(1–2), 93–111.

Kenyon, C. S., and L. R. Beddoes (1977), *Geothermal Gradient Map of Indonesia*, 50 pp., Indonesian Petroleum Association, Southeast Asia Petroleum Exploration Society, Jakarta.

Ketcham, R. A. (2005), Forward and inverse modeling of low-temperature thermochronometry data, *Rev. Miner. Geochem.*, *58*, 275–314.

Ketcham, R. A., R. A. Donelick, and W. D. Carlson (1999), Variability of apatite fission-track annealing kinetics: III. Extrapolation to geological time scales, *Am. Mineral.*, *84*(9), 1235–1255.

Leier, A., N. McQuarrie, C. Garzione, and J. Eiler (2013), Stable isotope evidence for multiple pulses of rapid surface uplift in the Central Andes, Bolivia, *Earth Planet. Sci. Lett.*, *371-372*, 49–58.

Lourens, L. J., F. J. Hilgen, N. J. Shackleton, J. Laskar, and D. Wilson (2004), The Neogene period, in *Geological Time Scale*, edited by F. M. Gradstein, J. G. Ogg, and A. G. Smith, pp. 409–440, Cambridge Univ. Press, Cambridge.

Mccaffrey, R., P. Molnar, S. W. Roecker, and Y. S. Joyodiwiryo (1985), Microearthquake seismicity and fault plane solutions related to arc-continent collision in the eastern Sunda Arc, Indonesia, *J. Geophys. Res.*, *90*(Nb6), 4511–4528, doi:10.1029/JB090iB06p04511.

Meulenkamp, J. E., G. J. Vanderzwaan, and W. A. Vanwamel (1994), On late Miocene to recent vertical motions in the Cretan segment of the Hellenic Arc, *Tectonophysics*, *234*(1–2), 53–72.

Nguyen, N., B. Duffy, J. Shulmeister, and M. Quigley (2013), Rapid Pliocene uplift of Timor, *Geology*, *41*, 179–182.

Nugroho, H., R. Harris, A. W. Lestariya, and B. Maruf (2009), Plate boundary reorganization in the active Banda Arc-continent collision: Insights from new GPS measurements, *Tectonophysics*, *479*(1–2), 52–65.

O'Brien, G. W., M. Lisk, I. Duddy, P. J. Eadington, S. Cadman, and M. Fellows (1996), Late Tertiary fluid migration in the Timor Sea: A key control on thermal and diagenetic histories?, *APPEA J.*, *36*, 399–427.

Poage, M. A., and C. P. Chamberlain (2001), Empirical relationships between elevation and the stable isotope composition of precipitation and surface waters: Considerations for studies of paleoelevation change, *Am. J. Sci.*, *301*(1), 1–15.

Prasetyadi, C., and R. Harris (1996), Structure and tectonic significance of the Aileu formation East Timor, Indonesia, *Proceedings of the 25th Annual Convention of the Indonesian Association of Geologists*, 144-173.

Reiners, P. W. (2005), Zircon (U-Th)/He thermochronometry, *Rev. Miner. Geochem.*, *58*, 151–179.

Reiners, P. W., and M. T. Brandon (2006), Using thermochronology to understand orogenic erosion, *Annu. Rev. Earth Planet. Sci.*, *34*, 419–466.

Reiners, P. W., T. A. Ehlers, S. G. Mitchell, and D. R. Montgomery (2003), Coupled spatial variations in precipitation and long-term erosion rates across the Washington Cascades, *Nature*, *426*(6967), 645–647.

Reiners, P. W., T. L. Spell, S. Nicolescu, and K. A. Zanetti (2004), Zircon (U-Th)/He thermochronometry: He diffusion and comparisons with (40)Ar/(39)Ar dating, *Geochim. Cosmochim. Acta*, *68*(8), 1857–1887.

Robbins, G. A. (1972), *Radiogenic Argon Diffusion in Muscovite Under Hydrothermal Conditions*, 42 pp., Brown University, Providence, R. I.

Roosmawati, N., and R. Harris (2009), Surface uplift history of the incipient Banda arc-continent collision: Geology and synorogenic foraminifera of Rote and Savu Islands, Indonesia, *Tectonophysics*, *479*(1–2), 95–110.

Sandiford, M. (2008), Seismic moment release during slab rupture beneath the Banda Sea, *Geophys. J. Int.*, *174*(2), 659–671.

Sawyer, R. K., K. Sani, and S. Brown (1993), The stratigraphy and sedimentology of West Timor, Indonesia, paper presented at Proceedings Indonesian Petroleum Association.

Spakman, W., and R. Hall (2010), Surface deformation and slab-mantle interaction during Banda arc subduction rollback, *Nat. Geosci.*, *3*(8), 562–566.

Standley, C. E., and R. Harris (2009), Tectonic evolution of forearc nappes of the active Banda arc-continent collision: Origin, age, metamorphic history and structure of the Lolotoi Complex, East Timor, *Tectonophysics*, *479*(1–2), 66–94.

Tate, G. W., N. McQuarrie, R. Bakker, D. J. J. Van Hinsbergen, and R. Harris (2010), Active arc-continent accretion in Timor-Leste: New structural mapping and quantification of continental subduction, Abstract #*T51A-1996* presented at 2012 Fall Meeting, AGU, San Francisco, Calif., 13–17 Dec.

Timor-Leste Ministry of Agriculture, F. a. F. (2012), Climate and hydrology, edited.

Valenza, J. M., R. Harris, C. J. Spencer, C. W. Hoiland, and J. A. Flores (2013), Structure dynamics of the Banda Arc collision zone: Geochemical and Age analysis of ultramafic and mafic bodies in Timor, Indonesia, paper presented at AGU Fall Meeting, San Francisco, Calif.

Van der Zwaan, G. J., F. J. Jorissen, and H. C. De Stigter (1990), The depth dependency of planktonic/benthonic foraminiferal ratios: Constraints and applications, *Mar. Geol.*, *95*, 1–16.

van Hinsbergen, D. J. J., T. J. Kouwenhoven, and G. J. van der Zwaan (2005), Paleobathymetry in the backstripping procedure: Correction for oxygenation effects on depth estimates, *Palaeogeogr. Palaeoclimatol. Palaeoecol.*, *221*(3–4), 245–265.

Van Marle, L. J. (1988), Bathymetric distribution of benthic foraminifera on the Australian-Irian Jaya continental margin, eastern Indonesia, *Mar. Micropaleontol.*, *13*, 97–152.

Van Marle, L. J. (1989), Recent and fossil benthic foraminifera and late Cenozoic paleobathymetry of Seram, eastern Indonesia, *Neth. J. Sea Res.*, *24*(4), 445–457.

Van Marle, L. J. (1991), Eastern Indonesian, late Cenozoic smaller benthic foraminifera, *Mem. R. Dutch Acad. Sci. Phys. Div.*, *1*(34), 328.

Van Marle, L. J., J. E. Van Hinte, and J. Nederbragt (1987), Plankton percentage of the foraminiferal fauna in seafloor samples from the Australian-Irian Jaya continental margin, eastern Indonesia, *Mar. Geol.*, *77*, 151–156.

Wade, B. S., P. N. Pearson, W. A. Berggren, and H. Palike (2011), Review and revision of Cenozoic tropical planktonic foraminiferal biostratigraphy and calibration to the geomagnetic polarity and astronomical time scale, *Earth Sci. Rev.*, *104*(1–3), 111–142.

Willett, S. D. (1999), Orogeny and orography: The effects of erosion on the structure of mountain belts, *J. Geophys. Res.*, *104*(B12), 28,957–28,981, doi:10.1029/1999JB900248.

Willett, S. D., and M. T. Brandon (2013), Some analytical methods for converting thermochronometric age to erosion rate, *Geochem. Geophys. Geosyst.*, *14*, 209–222, doi:10.1029/2012GC004279.

Zobell, E. (2007), Origin and tectonic evolution of Gondwana sequence units accreted to the Banda Arc: A structural transect through central East Timor, 83 pp., Masters Thesis, Brigham Young University.